

1 **Late Glacial-Holocene tephra from southern Patagonia and Tierra del Fuego (Argentina,**
2 **Chile): a complete textural and geochemical fingerprinting for distal correlations in the**
3 **Southern Hemisphere**

4

5 Paola Del Carlo^a, Alessio Di Roberto^a, Massimo D’Orazio^b, Maurizio Petrelli^c, Andrea Angioletti^b,
6 Giovanni Zanchetta^{a,b}, Valter Maggi^d, Romina Daga^e, Manuela Nazzari^{f,g}, Sergio Rocchi^b

7

8 *a. Istituto Nazionale di Geofisica e Vulcanologia, Sezione di Pisa, Via della Faggiola 32, 56126*
9 *Pisa, Italy*

10 *b. Dipartimento di Scienze della Terra, Università di Pisa, Via Santa Maria, 53, 56126 Pisa, Italy*

11 *c. Dipartimento di Fisica e Geologia, Università di Perugia, Via A. Pascoli, I-06123 Perugia, Italy*

12 *d. Dipartimento Scienze dell'Ambiente e Territorio, Università degli Studi di Milano-Bicocca*
13 *Piazza della Scienza, 1, 2016, Milano, Italy*

14 *e. Laboratorio de Análisis por Activación Neutrónica, Centro Atómico Bariloche, 8400 Bariloche,*
15 *Argentina; Centro Científico Tecnológico - CONICET - Patagonia Norte, Av. de los Pioneros*
16 *2350, 8400 Bariloche, Argentina*

17 *f. Istituto Nazionale di Geofisica e Vulcanologia, Sezione di Roma1, Via di Vigna Murata 605,*
18 *00143, Roma, Italy*

19 *g. Dipartimento di Scienze della Terra, Sapienza Università di Roma, Piazzale Aldo Moro 5, Roma,*
20 *Italy*

21 **Corresponding author** Paola Del Carlo paola.delcarlo@ingv.it

22

23 **Keywords:** *Tephra, South America, Patagonia and Tierra del Fuego, Explosive volcanism,*
24 *Holocene, Hudson volcano, Mt Burney volcano, Reclus volcano, Antarctica*

25 **1. Abstract**

26 Explosive volcanoes from the southern Andes are able to disperse ash over wide areas of the
27 Southern Hemisphere, potentially as far as Antarctica. With the aim of improving correlations
28 between sources and tephra in southernmost South America and, possibly, Antarctica, this work
29 presents new field, textural and geochemical data on tephra layers from southern Patagonia and
30 Tierra del Fuego (Argentina and Chile). Major- and trace-element data, obtained on single glass
31 shards allowed to identify tephra sources in Late Glacial-Holocene eruptions from Hudson, Reclus
32 and Mt Burney volcanoes, located in the Southern and Austral Volcanic Zone of the Andean
33 Cordillera. Twelve new radiocarbon age determinations of charcoals, peats and soils have further
34 constrained the correlations between the studied tephra layers and known eruptions from Hudson, Mt
35 Burney and Reclus volcanoes. Therefore, this study contributes to expand the geochemical dataset on
36 volcanic glasses valuable for tephra correlations in South America, and improves the current
37 tephrostratigraphic framework of this region. Furthermore, we revised literature data by compiling a
38 database including Neogene-Quaternary volcanic tephra found in Antarctic ice cores, marine
39 sediments, blue ice and continental outcrops as well as tephra produced by volcanic sources located
40 in Antarctica and circum-Antarctic areas. This revision shows that Antarctic tephra can be correlated
41 with confidence to Antarctic and circum-Antarctic (South Shetlands and South Sandwich Islands)
42 volcanic sources, whereas correlations with South American sources are arguable, and a complete
43 geochemical fingerprinting is needed for validation.

44

45

46

47

48

49

50 **2. Introduction**

51 Tephra layers preserved in geological records represent a valuable tool for reconstructing the past
52 volcanic activity of a given area. Moreover, they are isochronous marker horizons providing time-
53 stratigraphic information whenever they are geochemically fingerprinted and tied to a known, dated
54 eruption (Lowe, 2011; Lowe and Alloway, 2015). Volcanoes of southernmost South America have
55 been proposed as possible extra-Antarctic sources of some tephra recovered in Antarctic glacial
56 archives (Kurbatov et al., 2006; Narcisi et al., 2010; Narcisi et al., 2012), along with those from the
57 South Sandwich Islands and New Zealand (Dunbar et al., 2017; Narcisi et al., 2005; Narcisi et al.,
58 2012). Thus, in this perspective, tephra recovered from southern Patagonia and Tierra del Fuego
59 (hereafter SPTF) have additional value as a tool for the correlation of geological, paleoclimatic and
60 paleoenvironmental archives at intercontinental scale.

61 Late Glacial to Holocene tephra layers in SPTF (Argentina and Chile) have been recovered in
62 different sedimentary archives including terrestrial outcrops, marine and lacustrine cores (Fontijn et
63 al., 2014). They have been produced by several volcanoes during tens of eruptions some of which are
64 characterized by intensities up to a Volcanic Explosive Index (VEI) of 6 (Naranjo and Stern, 1998).
65 Some of these eruptions emplaced volumes of tephra larger than 20 km³ (e.g., Hudson Ho eruption;
66 Weller et al., 2014), with a dispersal area covering almost the whole SPTF and extending over the
67 surrounding oceans.

68 Despite their significance, and with the exception of few cases (Haberle and Lumley, 1998; Kilian et
69 al., 2003; Kratzmann et al., 2010; Stern, 2008; Weller et al., 2014), most of the eruptions occurred in
70 the SPTF have been solely characterized by the chemical composition of the bulk tephra deposit or
71 the bulk rock analysis of the juvenile component. Conversely, textural and mineralogical
72 characterization, as well as major- and, even most, trace-element analyses of glasses are scarce. This
73 issue represents a significant limitation when correlating tephra at both proximal to distal scale (i.e.,
74 SPTF) and distal to ultra-distal, Southern Hemisphere-wide scale (e.g., with the Antarctic ice
75 records). In fact, the major- and trace-element compositions of the bulk deposit may significantly
76 differ from that of individual glass shards, commonly recovered and analyzed in ultra-distal

77 locations, since the former may be variably affected by sample heterogeneity, and inter-shard
78 variations (Pearce et al., 2004). Moreover, the bulk rock composition will correspond to that of glass
79 fraction only if the first one is aphyric and formed only by juvenile material with no accidental
80 lithics. Finally, many explosive eruptions are rhyolitic or dacitic in composition and almost
81 indistinguishable using the major-element chemistry alone. In such cases, the study of textural and
82 mineralogical features of tephra (e.g., nature and abundance of the components, particles
83 morphology, vesicle size and distribution and crystal content) associated with single-glass-shard
84 trace-element data is an invaluable help for the identification of their eruptive sources and for the
85 correlation of different tephra layers (Pearce et al., 2004). This approach, typical of modern
86 tephrostratigraphy, has never been fully applied to Patagonian tephra and only few papers report on
87 the textural and physical features of studied deposits as well as on the mineralogical assemblage of
88 distal tephra.

89 In this work, we present and discuss new data on texture, mineralogy, major- and trace-element
90 geochemical composition performed on single glass shards of several tephra layers occurring in
91 different, mostly unreported, stratigraphic sections in SPTF (Argentina and Chile). In addition, we
92 provide new radiocarbon ages of charcoals, peats, and soils that further constrain the correlation
93 between tephra layers and known volcanic eruptions. Findings of this investigation implement the
94 existing tephrostratigraphic framework for the SPTF by also increasing the inventory of known
95 outcrops. In the light of these results, we discuss the provenance of some tephra layers found in the
96 Antarctic ice-records and previously attributed to the volcanoes of Southern and Austral Volcanic
97 Zone of the Andean Cordillera.

98

99

100

101 **3. Volcanological framework**

102 In South America, most of the explosive Holocene volcanism is produced by the Andean Arc, a
103 segmented volcanic arc along the Andean Cordillera (Stern, 2004). Volcanism formed as a result of
104 the subduction of the Nazca and Antarctic plates underneath the South American Plate (Fig. 1), and
105 is subdivided into four main volcanic zones separated from each other by volcanic gaps (Stern et al.,
106 1984): the Northern (NVZ), the Central (CVZ), the Southern (SVZ), and the Austral Volcanic Zone
107 (AVZ). The SVZ and AVZ are the closest to the area under study.

108 The SVZ comprises 60 volcanic centers aligned along a 1400 km-long, continuous volcanic arc
109 active since the Late Quaternary. Similarly, the AVZ volcanic arc comprises six volcanic complexes
110 active since the Late Quaternary: Lautaro, Viedma, Aguilera, Reclus, Mt Burney and Fuego, also
111 known as Cook (Corbella and Lara, 2008; Stern and Kilian, 1996).

112 Tephrostratigraphic and tephrochronological studies conducted in the Patagonia-Tierra del Fuego
113 region have shown that explosive volcanism has been extremely active during the Holocene and Late
114 Glacial period, often with high magnitude eruptions (Fontijn et al., 2014). In geological records,
115 tephra layers have been correlated to large eruptions from four principal sources: Hudson, Mt
116 Burney, Reclus and Aguilera volcanoes (Stern, 2008; Fig. 1).

117 The Hudson volcanic complex is the most active in the southern SVZ. Tephrostratigraphic records
118 count at least a dozen of large-scale explosive eruptions since the Late Glacial period (Fontijn et al.,
119 2014). The major explosive events of Hudson volcano occurred at ca. 17,400 cal yrs BP (Ho) (Weller
120 et al., 2014), at 7,750 cal yrs BP (H₁) (Fontijn et al., 2014; Prieto et al., 2013), at 3,920 cal yrs BP
121 (H₂) (Naranjo and Stern, 1998), and in AD 1991 (H₃) (Scasso et al., 1994). All these eruptions
122 produced a considerable volume of pyroclastic material, possibly ranging between >20 km³ (Ho) to
123 ca. 4.3 km³ (H₃).

124 Mt Burney is a volcanic complex formed by a somma and an inner stratocone. The study of tephra
125 over the Patagonia and Tierra del Fuego has yielded evidence for several eruptions from Mt Burney
126 volcano, including two large Plinian eruptions named MB₁ and MB₂ (Stern, 2008). Radiocarbon
127 dating indicates an age for MB₁ eruption comprised between 8,851 and 9,949 cal yrs BP (Kilian et

128 al., 2003; Stern, 2008). The age of MB₂ tephra has also been determined at several sites between
129 3,818 and 4,711 cal years BP (Kilian et al., 2003; McCulloch and Bentley, 1998; McCulloch and
130 Davies, 2001; Stern, 2008). Both the Plinian eruptions producing MB₁ and MB₂ tephra were VEI 5
131 and produced volumes of tephra exceeding 3 and 2.8 km³, respectively (Stern et al., 2008). Some
132 other minor tephra layers have been identified possibly emplaced after smaller eruptions of Mt
133 Burney (Kilian et al., 2003). These have been dated from the oldest to the youngest at >9,511 cal yrs
134 BP, between 9,175±111 and 9,511±121 cal yrs BP and between 2,026±48 to 2,063±90 cal yrs BP
135 (Kilian et al., 2003).

136 Reclus is a small stratovolcano that has erupted mainly dacite lavas and pyroclastic ejecta
137 (Harambour, 1988). The present tephrostratigraphic and tephrochronologic framework in southern
138 Patagonia points to three main tephra layers sourced from Reclus volcano. The widespread R₁ tephra
139 layer (Tephra I of Auer, 1974) is attributed to a Plinian eruption of Reclus volcano dated at ~12,700
140 ¹⁴C yrs BP (McCulloch and Davies, 2001; McCulloch et al., 2005; Stern, 2008; Stern et al., 2011)
141 and possibly involving a volume of ca. 5 km³ of pyroclastic material (Stern et al., 2011). Several
142 other Holocene tephra layers chemically compatible with Reclus volcano, but much thinner and
143 considerably less spatially dispersed than R₁, have been identified in several localities of southern
144 Patagonia. In particular, two tephra, R₂ and R₃, derived from Reclus have been found in sediment
145 cores from Torres del Paine National Park, southern Chile (Villa-Martínez and Moreno, 2007) and
146 have been dated at 1789 cal yrs BP and 1035 cal yrs BP, respectively (Breuer et al., 2013; Moy et al.,
147 2008).

148 Aguilera is a remote stratovolcano identified in 1985 and indicated as the source of a regionally
149 widespread Holocene tephra named A₁, mostly found close to Lago Argentino just east of this
150 volcano. The A₁ tephra has an estimated age of ~3,067-3,339 cal yrs BP (Stern, 2008). Several other
151 thinner and less widely distributed tephra layers have been identified in the vicinity of Lago
152 Argentino and Torres del Paine, and correlated to Aguilera volcano. The age obtained for one of

153 these layers is older than the age of A₁ tephra layer around <4,560 ¹⁴C yrs BP. The age of tephra
154 layers younger than A₁ was not constrained.

155 The three remaining volcanoes of the AVZ, namely Lautaro, Viedma, and Fueguino (Fig. 1) erupted
156 in the Holocene and during historical time. Lautaro and Viedma are two stratovolcanoes located in
157 the northernmost AVZ (Corbella and Lara, 2008), yet no tephra layers in SPTF have attributed to
158 their activities. Fueguino represents the southernmost Holocene volcanic occurrence of the Andes
159 (Corbella and Lara, 2008). It produced a cluster of small pyroclastic cones (<150 m) and columnar-
160 jointed lava domes (Puig et al., 1984); this small to moderately energetic activity makes unlikely that
161 widely dispersed tephra sourced from this complex.

162

163 **4. Sampling and Methods**

164 Stratigraphic logging and sampling of tephra layers were performed (February 2015 field work) in
165 SPTF (Fig. 1 and Table 1 for coordinates of stratigraphic sections). Sampling sites have been
166 selected in medial-distal locations, with respect to the potential Holocene volcanic sources of tephra,
167 and following criteria of easy accessibility and good exposure of the outcrops. From north to south,
168 the stratigraphic sections here reported are: Arroyo Robles close to the Potrok Aike Lake (Argentina;
169 section AR-1), Río Rubens (Argentina; section RR-1), Estancia Otway (Chile; sections EO-1, EO-2),
170 Río O'Higgins (Tierra del Fuego, Chile; section ROH-2); Punta Arenas (Chile; section PA-1), Río
171 Tres Brazos (Chile; sections RTB-1, RTB-2), Laguna de los Cisnes (Tierra del Fuego, Chile; section
172 LA-1). These are all unreported outcrops but one (ROH-2) (Stern, 1991). Tephra layers with a
173 thickness ranging from 1 to 16 cm have been identified mainly in natural exposures including banks
174 of alluvial and meandering channels, peat bogs, alluvial terraces, as well as in trenches dug for
175 livestock beverage and road cuts, yielding 16 samples.

176 Samples were first washed with deionized water in an ultrasonic bath to disaggregate them and to
177 remove impurities. Hydrochloric acid (10% v/v) was added to the samples to dissolve carbonates.
178 Afterward, hydrogen peroxide (35% v/v) was repeatedly added to the samples that were successively

179 heated at 120°C to further disaggregate the matrix, remove organic matter and soluble compounds.
180 Samples were then dried at 60°C, mounted with epoxy resin in 1-inch stubs, polished and prepared
181 for textural and geochemical analyses.

182 Tephra samples were described under a petrography microscope. The texture, components and
183 mineral assemblage of tephra were studied at the Istituto Nazionale di Geofisica e Vulcanologia,
184 Sezione di Pisa (INGV-Pisa) with a scanning electron microscope (SEM) Zeiss EVO MA and
185 images have been collected in back-scattered electrons (BSE) mode. Major-element glass
186 compositions were determined at the Laboratorio Microsonda Elettronica C.N.R.-I.G.G. of Florence
187 using a JEOL JXA-8600 microprobe (EMP) equipped with 4 wavelength dispersive spectrometers
188 (operating conditions: 15 kV accelerating voltage, 10 nA beam current, 10 µm probe diameter and 20
189 s (10 s for Na and 40 s for Cl and F) and 20 s acquisition time for peak and background (40 s for Cl
190 and F), respectively) and at HPHT Laboratory INGV-Roma using a JEOL JXA 8200 electron
191 microprobe (EPMA) equipped with five wavelength-dispersive spectrometers (operating conditions:
192 15 kV accelerating voltage, 8 nA beam current, 5 µm probe diameter, 10 and 5 s acquisition time for
193 peak and background, respectively). Standards of glass and natural mineral phases were analyzed to
194 test the accuracy of data during the analyses (see Supplementary Material 1).

195 The trace-element concentrations were determined on single glass shards by Laser Ablation-
196 Inductively Coupled Plasma-Mass Spectrometry (LA-ICP-MS) at the Università di Perugia,
197 Dipartimento di Fisica e Geologia. The analyses were carried out with a Teledyne Photon Machine
198 G2 laser ablation system coupled to a Thermo Fisher Scientific iCAP-Q, quadrupole based, ICP-MS
199 (Petrelli et al., 2016a, 2016b; Petrelli et al., 2008). The LA-ICP-MS operating conditions were
200 optimized before each analytical session by continuous ablation of NIST SRM 612 glass reference
201 material (Pearce et al., 1997) to provide maximum signal intensity and stability for the ions of
202 interest while suppressing oxides formation (ThO^+/Th^+ below 0.5%). The U/Th ratio was also
203 monitored and maintained close to 1. The stability of the system was evaluated on ^{139}La , ^{208}Pb , ^{232}Th ,
204 and ^{238}U by a short-term stability test. It consisted of 5 acquisitions (one minute each) on a linear

205 scan of NIST SRM 612 glass reference material (Petrelli et al., 2016a, 2016b). Tephra glasses were
206 analyzed by using a circular laser beam with a diameter of 20 μm , a frequency of 8 Hz, and an
207 energy density at the sample surface of 3.5 J/cm². NIST SRM 610 reference material (Pearce et al.,
208 1997) was used as the calibrator and ²⁹Si as the internal standard. USGS BCR2G reference material
209 was analyzed as unknown to provide a quality control (Jochum et al., 2005). Under these operating
210 conditions, precision and accuracy are better than 10 % for all the investigated elements (Petrelli et
211 al., 2008; Petrelli et al., 2016a, 2016b).

212 Age of tephra was obtained by ¹⁴C-AMS radiometric dating of organic matter (charcoal, soil and peat
213 samples) that are intercalated with tephra layers. Unfortunately, organic matter was present only in 9
214 of the studied sections. Analyses have been performed at the CIRCE laboratories, Caserta, Italy.
215 Radiocarbon dates were converted to calendar years before present (cal years BP) with the CALIB
216 7.01 program (Stuiver et al., 2018), using the IntCal13 radiocarbon ages calibration curve (Reimer et
217 al., 2013).

218

219 **5. Results: chemical composition, tephra texture, mineral assemblage and age**

220 A synoptic view of the features of the studied tephra layers is reported in Table 1 including grainsize,
221 nature and relative abundance of components, texture of volcanic particles and mineral assemblage.
222 Figures 2 and 3 report the photographs and the schematic representation of the studied stratigraphic
223 sections, respectively. Figures 4, 5 and 6 show selected SEM-BSE images of the studied tephra. The
224 major- and trace-element compositions of each sample are reported in Table 2 as averages of
225 multiple point analyses by EPMA and LA-ICP-MS, and the whole analytical data set is reported in
226 Supplementary Material 1.

227 The total alkali vs silica diagram (TAS, Fig. 7a; Le Bas et al., 1986) shows two main compositional
228 clusters for the glasses of the studied tephra in the trachyte and rhyolite fields, respectively. In detail,
229 samples EO-2H, EO-1B, ROH-2C and AR-F1 plot overall in the trachyte field, with SiO₂ ranging

230 between 63.7 and 68.6wt%. All the other samples plot into the rhyolite field with SiO₂ comprised
231 between 73.4 and 79.8 wt%.

232 In the K₂O vs SiO₂ diagram (Fig. 7b), which is commonly regarded as the most significant plot to
233 discriminate tephra from Patagonia and Tierra del Fuego (Stern, 2008), the samples form three main
234 compositional groups. The first one (Group Tr) consists of the four trachyte samples. The rhyolite
235 samples compositions define two distinct clusters. Among these, the Group Rh1 is characterized by a
236 SiO₂ ranging between 73.4 and 79.8 wt% and K₂O between 1.19 and 2.25 wt% (samples ROH-2B,
237 RTB-1B, EO-1C, EO-2D, EO-2L, AR-1B, AR-1D, RR-2B, and PA-1B). On the contrary, the Group
238 Rh2 shows more restricted SiO₂ values comprised between 77.1 and 78.4 wt% and higher K₂O,
239 ranging between 2.46 and 2.95 (samples EO-2B, RTB-2B, and LA-1B).

240 The distribution of the incompatible elements of the 16 samples analyzed by LA-ICP-MS (Fig. 8) is
241 that typical of orogenic magmas, with negative anomalies of Nb, Ta and Ti and positive anomalies of
242 Pb. However, some significant differences between samples belonging to groups Tr, Rh1 and Rh2
243 can be observed. On average Group Tr shows higher content for most incompatible elements than the
244 other two groups and particularly from Nd to Lu. Moreover, Rh1 glasses are less enriched in Rb than
245 those belonging to Groups Tr and Rh2 (Fig. 8).

246 These differences are emphasized in the diagrams Nb/Ba vs La/Zr, Rb/Ba vs Ti/Sm, Rb/Ba vs Sr/Nd
247 and Ce/Pb vs Ba/Th (Fig. 9). In these diagrams, samples belonging to Group Tr are well separated
248 from samples of groups Rh1 and Rh2. Indeed, these trachytes have distinctly higher Nb/Ba and
249 lower Sr/Nd and Ba/Th ratios. Rocks of Group Tr also have slightly higher Rb/Ba and Ce/Pb ratios.
250 The higher Nb/Ba and Ce/Pb ratios of Group Tr with respect to Groups Rh1 and Rh2 denotes a less
251 marked orogenic signature of the former. Groups Rh1 and Rh2 are less clearly discriminated from
252 each other, even though Rh1 samples have distinctly lower La/Zr and Rb/Ba, and higher Ba/Th with
253 respect to Rh2 samples. More in detail, the Rh1 samples PA-1B, RTB-1B, EO-1C and EO-2L have
254 lower La/Zr and higher Ti/Sm ratios, whereas samples RR-2B, AR-1B and AR-1D share higher

255 La/Zr and lower Ti/Sm ratios. Samples EO-2D and ROH-2B are characterized by intermediate
256 values of these trace element ratios (Fig. 9).

257 The textural features and the mineral assemblage of the studied samples (Table 1) are consistent with
258 the groups identified with the compositional data. In fact, Group Tr tephra are mainly composed of
259 blocky, y-shaped or platy-cusate, poorly-vesicular glass fragments (<100 μm) along with a minor
260 amount of micropumices with spherical to slightly elongated and deformed vesicles. They contain
261 scarce amounts of loose crystals of plagioclase (pl), orthopyroxene (opx), clinopyroxene (cpx),
262 quartz (qz) and apatite (ap) (Table 1).

263 Group Rh1, conversely, is mostly composed of highly- to moderately-vesicular micropumices with
264 spherical to coalesced and collapsed vesicles; micropumices occasionally bear microlites of pl, qz,
265 opx, cpx and Fe-Ti oxides (Table 1). Samples from Group Rh1 commonly contain also abundant
266 loose crystals of pl, qz, opx, Fe-Ti spinels and ap coated with volcanic glass (Table 1).

267 Group Rh2 is composed of moderately- to poorly-vesicular, blocky and y-shaped glass shards,
268 bubble walls and bubble junctions together with a minor amount of micropumices with tubular,
269 coalesced and collapsed vesicles (Table 1). Glass fragments are mostly aphyric with rare microlites
270 of pl, opx and ap. The tephra also contains scarce loose crystals of pl, opx and ap and holocrystalline
271 volcanic rock fragments (Table 1).

272 Radiocarbon ages obtained from studied successions are reported in Table 3. Ages span from Late
273 Glacial (EO-2A) to modern age (RR-2B), yet mostly comprised within the Holocene.

274

275 **6. Discussion**

276 **6.1. Sources of tephra**

277 To assess the volcanic provenance of the studied tephra, we compared their glass compositions with
278 those available in the literature. Moreover, we used the nature and abundance of components and the
279 texture of juvenile particles (e.g. particle shape, vesicularity, type and abundance of microlites)
280 forming pyroclastic deposits and the relevant constraints provided by radiocarbon ages.

281 It is worth to note that the geochemical characterization and provenance of tephra layers from
282 southern Andes volcanoes have been mainly performed through the analysis of the major-element
283 compositions on bulk tephra up to recent times. The use of trace elements to improve the success of
284 the identification process is scarce. Furthermore, major- and trace-element determinations on single
285 glass shards analyses are even rarer. These latter should be preferred to bulk analyses because bulk
286 tephra often contain abundant phenocrysts, volcanic-lithic fragments, and non-volcanic material, and
287 therefore may not represent the actual composition of the melt fraction quenched at the time of
288 eruption (Pearce et al., 2004), which is indeed represented by glass shards (Shane et al., 2008).
289 The comparison between our microprobe major-element data on glass shards and the only available
290 literature data (see references in the legend of Figs. 10 and 11) on glass shards and bulk tephra as
291 well, shows that the three compositional groups Tr, Rh1 and Rh2 match very well three volcanic
292 sources located in the Southern and Austral Volcanic Zone of the Andean Cordillera (Figs. 10 and
293 11): Hudson (Tr), Mt Burney (Rh1) and Reclus (Rh2) volcanoes.

294

295 *Compositional Group Tr - Hudson*

296 The major- and trace-element glass compositions of samples belonging to Group Tr closely match
297 that of tephra erupted by Hudson volcano during the Holocene (Figs. 10a and 11a,b). Radiocarbon
298 determinations constrain the age of Tr-tephra between $7,026 \pm 49$ and $4,219 \pm 241$ yrs BP (Figs. 3 and
299 12), suggesting they were most likely produced by the mid-Holocene H₁ eruption. This represents the
300 largest Holocene volcanic event of the southern Andes, with a volume of erupted materials $>18 \text{ km}^3$
301 (Naranjo and Stern, 1998; Stern, 2008) and an age of $7,750 \pm 95$ cal yrs BP obtained as the best
302 average among several samples from TF (Prieto et al., 2013). Thickness of tephra belonging to
303 Group Tr is fully compatible with that of tephra previously identified in the SPTF region and
304 correlated with H₁ eruption (Prieto et al., 2013).

305

306 *Compositional Group Rh1 - Mt Burney*

307 Major element glass composition of samples belonging to Group Rh1, which includes the majority of
308 the studied tephra, match that of the products erupted by Mt Burney volcano during the Holocene
309 (Fig. 10b). Within compositional Group Rh1, samples EO-2D, ROH-2B and AR-1D are well
310 bracketed in age between $9,299\pm 65$ and $7,325\pm 46$ yrs BP (Fig. 3). This age is compatible with the
311 age of MB₁ eruption which is dated either at 8,851-9,949 cal yrs BP (Stern, 2008) or in the range of
312 9,009-9,175 cal yrs BP (Kilian et al., 2003). The compositions of Group Rh1 match also those of
313 tephra layer 5022-2T1 identified between 12.32-12.34 m in the ICDP core 5022 from Laguna Potrok
314 Aike in southern Patagonia, Argentina, correlated with the MB₁ tephra layer from Mt Burney
315 (Wastegård et al., 2013). The age-depth model reported for the core (Kliem et al., 2013) indicates
316 that the tephra layer has an age of $\sim 9,545$ cal yrs BP (2σ range 8851–10238 cal yrs BP) which
317 overlaps the range reported for MB₁ eruption (Stern, 2008) (Fig.12). Thickness of studied tephra
318 layer is compatible with that of tephra layers attribute to MB₁ eruption and previously identified in
319 the SPTF region (Stern, 1991; Kilian et al., 2003; Stern, 2008).

320 Remarkably, in our Arroyo Robles section, a 2.5 cm thick tephra layer occurs under the MB₁ tephra
321 separated by a 2 cm-thick peat horizon (Fig. 3). This tephra (AR-1B) has the same petro-chemical
322 characteristics (Fig. 9) of the overlying MB₁ tephra (AR-1D) and can be attributed to an explosive
323 activity of the Mt Burney slightly older than MB₁. Several pre-MB₁, tephra layers, dated between
324 ~ 20 and ~ 50 ka, have been identified in the Laguna Potrok Aike lacustrine record (Wastegård et al.,
325 2013) and attributed to Mt Burney activity. Accordingly, tephra AR-1B could represent the first
326 report of a Mt Burney eruption occurred between MB₁ and the those documented in the Potrok Aike
327 record.

328 The age of the rest of Group Rh1 samples (EO-2L, EO-1C, PA-1B, RR-2B, and RTB-1B) is not fully
329 constrained. We obtained a maximum age of $4,219\pm 241$ yrs BP from a sample at the very base of
330 sample EO-2L, but no age constraints at the top (Figs. 2, 3 and 12). In this regard, we do not observe
331 any evidence of a sedimentological break or hiatus occurring between the dated peat sample and EO-
332 2L tephra. EO-2L can be thus correlated with the Mid-Holocene Plinian eruption MB₂ of Mt Burney

333 volcano dated 3,818-4,711 cal yrs BP (Kilian et al., 2003; McCulloch and Bentley, 1998; McCulloch
334 and Davies, 2001; Stern, 2008). Similarly, sample EO-1C is separated by a few cm of sediment from
335 EO-1B tephra (Figs. 2 and 3), which is in turn correlated with the Hudson H₁ eruption dated at
336 7,750±95 cal yrs BP (Prieto et al., 2013). The age of the tephra EO-1C is thus younger than the age
337 of H₁ allowing a possible correlation to MB₂ eruption from Mt Burney, that in the investigated area
338 is reported to reach 5 cm of thickness (Stern, 2008), which is compatible with the 2-4 cm thickness
339 reported here. For PA-1B tephra, we obtained only a minimum age of 1,259±32 cal yrs BP, whereas
340 for RTB-1B tephra a modern age (Figs. 3 and 12). The RTB-1B age, however, is not coherent with
341 the stratigraphic framework, thus suggesting a considerably older age for this eruption. In addition,
342 we observe that samples PA-1B and RTB-1B have the same textural, mineralogical and
343 compositional characteristics as samples EO-2L and EO-1C (Fig. 10b). Thus we suggest their
344 correlation with MB₂ eruption.

345 Finally, sample RR-2B, which presents trace elements ratios different from EO-2L, EO-1C, PA-1B,
346 RTB-1B samples (Fig. 9) and a very young age (<200 yrs), may be correlated to the only known
347 historical eruption of Mt Burney occurred in 1910.

348 Comparing our compositional data for Mt Burney products with those available in the literature, we
349 observe a good correspondence with major-element compositions but not for trace-element
350 compositions (Fig. 11c and d). For instance, we observe a shift toward lower Rb content and a higher
351 Sr content in the literature data with respect to our compositions. This can be explained with the
352 different type of analyses performed: bulk-tephra and glass trace-element compositions determined
353 via energy dispersive XRF analysis (Stern, 2008; Stern and Kilian, 1996) could be affected by the
354 occurrence of microlites/crystals/lithics, whereas space-resolved single-shards LA-ICP-MS are
355 definitely representative of glass.

356

357 *Compositional Group Rh2 - Reclus*

358 Rhyolitic tephra of Group Rh2 can be correlated to the products erupted by Reclus volcano (Fig.
359 10c). In this case, the ¹⁴C ages indicate two sub-groups, i.e., samples EO-2B and RTB-2B with age
360 bracketed between 12,240±54 cal yrs BP and 9,299±65 cal yrs BP and LA-1B that is considerably
361 much younger and has an age of <3,264±46 cal yrs BP.

362 The first sub-group (samples EO-2B, RTB-2B) is compatible in age with R₁ eruption from Reclus
363 volcano that was dated between ca 12,700 yrs BP (McCulloch et al., 2005; Stern, 2008). Also the
364 thickness of EO-2B, RTB-2B tephra layers is compatible with that R₁ tephra which in this region is >
365 5 cm (Stern, 2008). As mentioned above, sample LA-1B is considerably much younger and has an
366 age of <3,385-3,585 cal yrs BP. This tephra is thus compatible in age with eruptions R₂ or R₃ dated
367 at 2,000 cal yrs BP (Villa-Martínez and Moreno, 2007). The two groups have very similar trace-
368 element signatures (Figs. 11e,f) apart from those compositions deriving from bulk analyses for the
369 reasons above explained.

370 Samples EO-2B, RTB-2B of Group Rh2 match also the composition of tephra layers 5022-2T2,
371 5022-2T3, and 5022-2T4 recovered at 16.04-16.05 m, 16.48 m and 16.78-16.79 m in the Laguna
372 Potrok Aike 5022 core and correlated with the Reclus R₁ tephra (Haberzettl et al., 2007; Wastegård
373 et al., 2013).

374

375 **6.2. South American tephra in Antarctica?**

376 Southern Andes volcanoes, along with New Zealand and South Sandwich Islands volcanoes have
377 been considered as potential sources for some Holocene ultra-distal tephra found in ice records at
378 various sites of Antarctica (Dunbar et al., 2017; Kurbatov et al., 2006; Narcisi et al., 2010). Detecting
379 whether these tephra layers are sourced from (i) mid-latitude volcanoes in the southern Andes or
380 New Zealand, (ii) mid/high-latitude circum-antarctic volcanic islands (South Sandwich and South
381 Shetlands) or (ii) high-latitude Antarctic volcanoes, is crucial to understand the atmospheric
382 circulations able to transport tephra onto the Antarctic ice. In this perspective, it urges a detailed
383 textural, mineralogical and geochemical fingerprinting, including major- and trace-element data of

384 tephra layers, in both ultra-distal and proximal-medial sites. This will offer a solid dataset in the
385 framework of which possible stratigraphic correlations among different geological archives would be
386 much more straightforward and reliable. To date, such a dataset is missing, while data are available
387 on the major-element glass composition and on the age of tephra layers based on glacial proxies.

388 On these bases, it is only possible to define compositional lineages in order to distinguish the main
389 sources of Antarctic tephra. To this aim, we collected major-element data of Neogene-Quaternary
390 tephra from Antarctic ice cores, marine sediments, blue ice, continental outcrops as well as for
391 potential sources located in Antarctica and circum-Antarctic areas (Supplementary Material 2). Then,
392 we critically reviewed the obtained dataset discarding any analysis showing evidence of alterations.
393 In detail, we applied the screening methods for altered specimens reported for Antarctic tephra (Di
394 Roberto et al., 2012), also considering the criteria of alteration and alkali loss (Kilian et al., 2003).
395 Figure 13 reports more than 2000 analyses in the widely used K_2O vs SiO_2 plot where the glass
396 compositions define six clear geochemical lineages.

397 Lineage 1 is a typical alkaline lineage (Fig. 13); this includes glasses erupted by intraplate alkaline
398 volcanoes of the West Antarctic rift system (e.g., McMurdo Volcanic Group, Marie Byrd Land
399 volcanoes), most of the Andrill samples (Miocene to Quaternary), and marine and englacial tephra
400 from Antarctica. At higher K_2O/SiO_2 relative to Lineage 1, nephelinites (1a) and phonolites (1b) are
401 found. A scarcely populated trend is defined by high-silica glasses, with alkali-rhyolite to pantellerite
402 compositions deriving from extreme fractionation of alkali feldspar and quartz ($SiO_2 > 70$ wt%,
403 Lineage 1c; Fig. 13) (Armienti et al., 1998; Armienti et al., 2001; Di Roberto et al., 2012; Martin et
404 al., 2010). Most of the tephra layers found in the Antarctic records show compositions that can be
405 correlated with alkaline products, typical of Antarctic alkaline volcanoes.

406 A limited number of Antarctic tephra shows a subalkaline, low-K tholeiitic to calc-alkaline, major-
407 element signature, typical of subduction zone igneous products. These tephra layers cannot be related
408 to the Antarctic alkaline volcanism, and can potentially derive from subduction-related volcanoes of
409 circum-Antarctic volcanic provinces, such as the Antarctic Peninsula area (South Shetland Islands),

410 the South Sandwich Islands in the southernmost Atlantic Ocean, the southern Andes and New
411 Zealand volcanic provinces (Fig. 13). These glass compositions define five other sub-alkaline
412 lineages.

413 Lineage 2 is potassic calc-alkaline (Fig. 13); this comprises glass compositions of tephra produced or
414 attributed to the Hudson volcano (including also four samples from this study). Also, Hudson
415 volcano has been proposed as the source for a trachybasaltic sample TD193 identified in the Talos
416 Dome core with an assigned age of 2.02 ka BP (Narcisi et al., 2012). This has been correlated to a
417 tephra with basaltic composition that is assumed to be regionally significant and bracketed between
418 uncalibrated radiocarbon ages $1,910 \pm 70$ and $2,235 \pm 130$ yrs BP (Naranjo and Stern, 1998). A few
419 Plinian eruptions fed by mafic magmas have been identified worldwide, able to spread ash to ultra-
420 distal sites, i.e., Etna 122 B.C. (Coltelli et al., 1998), Fontana Lapilli (ca. 60 ka BP), the Masaya
421 Triple Layer and the Masaya Tuff from Masaya caldera (2.1 and 1.8 ka BP), Nicaragua (Pérez et al.,
422 2009), and Tarawera, New Zealand in 1886 (Houghton and Gonnermann, 2008). For the Hudson
423 volcano, there is no evidence reported for such an eruption during the Late Glacial period and in the
424 Holocene, thus the correlation between TD193 tephra and Hudson volcano should be reconsidered.
425 Sample TD216, also from Talos Dome ice core, and dated $2,355 \pm 54$ yrs BP, has been correlated to
426 evolved products from Hudson, based on glass composition (Narcisi et al., 2012) slightly more
427 evolved than most evolved Hudson tephra. In the known volcanological record of this volcano, the
428 HW7 eruption has an age comparable to the one attributed to sample TD216 (Haberle and Lumney,
429 1998; Carel et al. 2011). However, the Ti content of TD216 tephra is significantly lower than that
430 present in Hudson samples with comparable SiO_2 , and also the ratios $\text{K}_2\text{O}/\text{TiO}_2$ and $\text{CaO}/\text{Al}_2\text{O}_3$ are
431 different. Therefore, the attribution of this tephra layer to Hudson volcano is not based on solid
432 ground.

433 Lineage 3 is rather K-rich calc-alkaline (Fig. 13) and includes the product erupted by Fueguino,
434 Macá, Cay, and Aguilera volcanoes and also the products from Antarctic Peninsula area (Seal
435 Nunataks) (Kraus et al., 2013). The glass compositions from Siple Dome ice core attributed to an

436 unreported eruption from Hudson volcano (Kurbatov et al., 2006), together with shards from Talos
437 Dome (Narcisi et al., 2012; Narcisi et al., 2017) ice cores, overlap the compositions of Aguilera
438 rhyolites. Nevertheless, these rhyolitic compositions also plot on the rhyolitic extension of the
439 Antarctic alkaline trend (Lineage 1c), and can therefore represent the extremely evolved alkaline
440 products of an Antarctic volcano. Tephra VK3311-2 and VK3311-4 from Vostok ice core have been
441 potentially attributed to a southern Andes or South Shetland source. Nevertheless, its rather old age
442 (414 ka) and the CaO and TiO₂ content make it difficult to correlate this tephra with either a Macá or
443 Cay source. Layers 1117.1 and 1868.3 from Dome C ice core have been attributed to a South
444 Shetland source (Narcisi et al., 2005) that, despite a rather low Al₂O₃ content, could be a plausible
445 correlation.

446 Lineage 4 is a rather K-poor calc-alkaline lineage (Fig. 13) that includes products erupted by the
447 Reclus volcano (Kilian et al., 2003; Stern and Kilian, 1996)(this work) and by volcanoes in the South
448 Shetlands and South Sandwich Islands. No shards from tephra recognized in Antarctic records plot
449 along this lineage, with the significant exception of a cryptotephra found in the WDC06A ice core,
450 recovered from central West Antarctica and attributed to the Oruanui supereruption from Taupo
451 volcano, at ca. 25.6 ka (Dunbar et al., 2017). Interestingly, the WDC06A ash layer has an average
452 composition closely matching that of Reclus tephra (Fig. 13). The only difference between WDC06A
453 ash layer and Reclus products is a pronounced spread in K₂O concentration (1.87 to 3.27 wt%), an
454 unusual feature for a strongly evolved, far-distal tephra. Tephra TD282 from Talos Dome ice core,
455 dated at 3,392±82 yrs BP (Narcisi et al., 2012) has K₂O vs SiO₂ relationships compatible with Reclus
456 compositions, but a correlation with Chile's Puyehue-Cordón Caulle has been suggested (Narcisi et
457 al., 2012). However, the K₂O/TiO₂ ratio (2.63) points out a composition far removed from typical
458 trends of southern Andes volcanoes for which the value of K₂O/TiO₂ expected at comparable SiO₂
459 content would be around 7, and overlapping instead South Shetlands compositions (Supplementary
460 Material 2).

461 Lineage 5 is a low-K tholeiitic trend (Fig. 13); this includes glass shards from Mt Burney and South
462 Sandwich Islands volcanic arc (Hubberten et al., 1991; Pearce et al., 2014). This lineage overlaps the
463 composition of some tephra layers found in Siple Dome, Vostok, and Talos Dome ice cores. Among
464 the latter, the majority of glass compositions with $\text{SiO}_2 < 70$ wt% is consistent with a provenance
465 from South Sandwich Islands (Basile et al., 2001). Conversely, glass with SiO_2 ranging between 70
466 and 75 wt%, cannot be definitively correlated with products of any known volcanic source. More in
467 detail, the SDMA2571 tephra in Siple Dome ice-core, dated at 1805 B.C., was related to the products
468 of Mt Burney (Kurbatov et al., 2006). According to these authors, the age of SDMA2571 tephra is
469 comparable to the MB₂ eruption from Mt Burney dated at 3,818-4,711 cal yrs BP (Kilian et al., 2003;
470 McCulloch and Bentley, 1998; McCulloch and Davies, 2001; Stern, 2008). However, the chemical
471 compositions of SDMA 2571 tephra do not match with the published composition of MB₂ eruption
472 tephra (Kilian et al., 2003; Stern, 2008; Wastegård et al., 2013). Our data also confirm this evidence.
473 In fact, although the glass composition of SDMA 2571 tephra lies on the compositional trend defined
474 by the Group Rh1 attributed to Mt Burney eruption, only a partial overlap exists between the most
475 evolved glass of SDMA2571 tephra and less evolved compositions measured in our samples (Fig.
476 13). In Talos Dome ice core, the cryptotephra layer TD299 dated at $3,677 \pm 92$ yrs BP was correlated
477 to this SDMA2571 tephra, thus in turn possibly correlated to the activity of Mt Burney, even though
478 not to a definite eruption. As reported for SDMA2571, no clear match exists between compositions
479 of TD299 tephra and products of Mt Burney eruptions (Kilian et al., 2003; Stern, 2008; Wastegård et
480 al., 2013) (Fig. 13). The glass composition with SiO_2 ranging between 70 and 75 wt% falling on this
481 trend and deriving from Antarctic ice records (mostly Siple Dome) can be correlated either with
482 evolved products from Mt Burney or with the most evolved compositions of the South Sandwich
483 Islands. Nevertheless, the drop in Al_2O_3 contents with increasing SiO_2 is not compatible with a Mt
484 Burney trend, making a South American source poorly feasible also in this case.

485 Also Lineage 6 is again a low-K tholeiitic lineage (Fig. 13), with a slightly lower K content and a
486 modest spread of SiO_2 concentrations than the Lineage 5. This lineage is defined by products of

487 South Sandwich Islands and Fueguino volcano. Tephra layers from Dome C, Siple Dome, Dome Fuji
488 and Vostok ice cores plot on this trend. In more detail, the andesitic layer 9008 from the Antarctic
489 SDMA (Siple Dome) ice core, dated 9,216 yrs B.C., and tentatively attributed to an eruption of the
490 Hudson volcano using geochemical and chronological data (Kurbatov et al., 2006), distinctively plot
491 on this trend (Fig. 13). Additionally, a Hudson tephra characterized by this composition and by a
492 large dispersion such as to justify its transport up to the Antarctic it is not known in Patagonia-Tierra
493 del Fuego. It is therefore plausible this tephra is sourced in South Sandwich volcanic activity.

494 The result of the comparison between our data and those available in the literature indicates that
495 Antarctic tephra mostly derives from Antarctic or circum-Antarctic volcanoes. For subalkaline
496 tephra, proposed correlations with South American volcanoes are either unfeasible or at least
497 alternative origins are equally feasible. In summary, for Holocene tephra found in Antarctica there is
498 no straightforward need to invoke a source at latitude lower than the circum-Antarctic volcanoes. A
499 possible exception could be represented by the cryptotephra found in WDC ice core correlated with
500 Oruanui supereruption, from Taupo (Dunbar et al., 2017). However, atmospheric dispersal modeling
501 indicates a significant ash accumulation of 30 g/m² on the core site (Dunbar et al., 2017), quite at
502 odds with the extremely fine grain-size of the cryptotephra and the convolute atmospheric path
503 followed by the particles arriving on site more than eight days after the eruption.

504 Possible explanations for the lack of South American tephra in Antarctica can be given in the light of
505 results recently published dealing with the potential ash impact from Antarctic volcanoes (Geyer et
506 al., 2017). Findings indicate that the potential impact of volcanic ash from Antarctic eruptions is
507 linked to volcano locations and eruption intensities. Eruptions with eruptive plumes <10 km in height
508 and from latitude >70° are likely to be confined in Antarctica due to moderated wind zones encircled
509 by the polar jet stream. Conversely, eruptive plumes >10 km in height have a higher potential for
510 extra-Antarctic ash dispersal. Also, eruptions from lower-latitude Antarctic volcanoes as Deception
511 Island are more likely to encircle the globe with ash, even for moderate size eruptions, reaching
512 tropical latitudes (Geyer et al., 2017). This because they are located out of the control of the polar jet

513 stream. The lack of ash produced by Austral mid-latitude volcanoes can be due to the effect of the
514 polar jet stream, which acts as a physical barrier on its two sides, hampering their dispersal to
515 Antarctica.

516

517

518

519 **7. Conclusions**

520 New field occurrences of tephra layers produced by Andean large-scale Holocene eruptions are
521 reported from SPTF. These findings considerably expand the present knowledge of the areal
522 dispersion of these tephra and offer new tie points for future precise eruption volume calculation. A
523 complete stratigraphic, geochronological (whenever possible), textural, mineralogical and
524 compositional characterization of tephra has been carried out including the determination of major
525 and trace elements on single glass shards by EPMA and LA-ICP-MS. These results significantly
526 strengthen the tephrostratigraphic framework of the Patagonia-Tierra del Fuego for the last ca. 13 ka
527 by applying, for the first time in this area, the multidisciplinary approach of the modern
528 tephrostratigraphy and tephrochronology. On this solid ground, we correlated tephra layers across the
529 studied stratigraphic sections and found the volcanic source of studied tephra layers in Hudson, Mt
530 Burney and Reclus volcanoes in the southern Andes. In detail, we correlate the tephra layers with
531 major explosive eruptions that affected SPTF during the Late Glacial to Holocene, namely the H₁
532 eruption from Hudson, MB₁ and MB₂ eruptions from Mt Burney and R₁ and R₂/R₃ eruptions from
533 Reclus.

534 We compiled a database including major- and trace-element compositional data of Neogene-
535 Quaternary tephra found in Antarctic ice cores, marine sediments, blue ice and continental outcrops
536 as well as tephra produced by volcanic sources located in Antarctica and circum-Antarctic areas. We
537 revised the chemical and petrological soundness of the attribution of some of these tephra to South
538 American volcanic sources. Results indicate that most, if not all, tephra layers identified in Antarctic

539 records can be correlated with Antarctic or circum-Antarctic volcanic sources (South Sandwich and
540 South Shetland Islands). No clear need exists to invoke South American volcanic sources. If
541 confirmed, this result calls for additional unequivocal new data to infer Holocene atmospheric
542 circulation and transport of tephra from mid-latitudes to Antarctica.

543

544 **Acknowledgements**

545 This research was funded by PNRA 2013/B2.10 project, PI S. Rocchi. This paper is sponsored by the
546 SCAR Expert Group, AntVolc. E. Braschi and A. Orlando are kindly acknowledged for their
547 assistance with the microprobe analyses at CNR-IGG laboratory in Florence. We also acknowledge
548 the Department of Physics and Geology, University of Perugia for the ‘CHALLENGE’ FRB 2015
549 grant (PI M. Petrelli). We are grateful to A. Geyer and an anonymous reviewer for their thorough
550 revision and constructive comments which led to significant improvement of the manuscript.

551

552 **References**

- 553 Armienti, P., Messiga, B., Vannucci, R., 1998. Sand provenance from major and trace element analyses of
554 bulk rock and sand grains. *Terra Antart.* 5, 589-599.
- 555 Armienti, P., Tamponi, M., Pompilio, M., 2001. Petrology and provenance of volcanic clasts, sand grains and
556 tephra. *Terra Antart.* 8, 2-23.
- 557 Basile, I., Petit, J.R., Touron, S., Grousset, F.E., Barkov, N., 2001. Volcanic layers in Antarctic (Vostok) ice
558 cores: Source identification and atmospheric implications. *Journal of Geophysical Research:*
559 *Atmospheres* 106, 31915-31931.
- 560 Breuer, S., Kilian, R., Baeza, O., Lamy, F., Arz, H., 2013. Holocene denudation rates from the superhumid
561 southernmost Chilean Patagonian Andes (53°S) deduced from lake sediment budgets. *Geomorphology*
562 187, 135-152.
- 563 Coltelli, M., Del Carlo, P., Vezzoli, L., 1998. Discovery of a Plinian basaltic eruption of Roman age at Etna
564 volcano, Italy. *Geology* 26, 1095-1098.
- 565 Corbella, H., Lara, L.E., 2008. Late Cenozoic Quaternary Volcanism in Patagonia and Tierra del Fuego, in:
566 Rabassa, J. (Ed.), *The Late Cenozoic of Patagonia* Elsevier, pp. 95-119.
- 567 Curzio, P., Folco, L., Ada Laurenzi, M., Mellini, M., Zeoli, A., 2008. A tephra chronostratigraphic framework for
568 the Frontier Mountain blue-ice field (northern Victoria Land, Antarctica). *Quat Sci Rev* 27, 602-620.
- 569 Del Carlo, P., Di Roberto, A., Vincenzo, G., Bertagnini, A., Landi, P., Pompilio, M., Colizza, E., Giordano, G.,
570 2015. Late Pleistocene-Holocene volcanic activity in northern Victoria Land recorded in Ross Sea
571 (Antarctica) marine sediments. *Bull. Volc.* 77, 1-17.
- 572 Del Carlo, P., Panter, K.S., Bassett, K., Bracciali, L., Di Vincenzo, G., Rocchi, S., 2009. The upper
573 lithostratigraphic unit of ANDRILL AND-2A core (Southern McMurdo Sound, Antarctica): Local
574 Pleistocene volcanic sources, paleoenvironmental implications and subsidence in the southern Victoria
575 Land Basin. *Global and Planetary Change* 69, 142-161.

576 Di Roberto, A., Del Carlo, P., Rocchi, S., Panter, K.S., 2012. Early Miocene volcanic activity and
577 paleoenvironment conditions recorded in tephra layers of the AND-2A core (southern McMurdo Sound,
578 Antarctica). *Geosphere* 8, 1342-1355.

579 Dunbar, N.W., Iverson, N.A., Van Eaton, A.R., Sigl, M., Alloway, B.V., Kurbatov, A.V., Mastin, L.G., McConnell,
580 J.R., Wilson, C.J.N., 2017. New Zealand supereruption provides time marker for the Last Glacial
581 Maximum in Antarctica. *Scientific Reports* 7, 12238.

582 Dunbar, N.W., Kurbatov, A.V., 2011. Tephrochronology of the Siple Dome ice core, West Antarctica:
583 correlations and sources. *Quat Sci Rev* 30, 1602-1614.

584 Dunbar, N.W., McIntosh, W.C., Esser, R.P., 2008. Physical setting and tephrochronology of the summit
585 caldera ice record at Mount Moulton, West Antarctica. *Geol. Soc. Am. Bull.* 120, 796-812.

586 Dunbar, N.W., Zielinski, G.A., Voisins, D.T., 2003. Tephra layers in the Siple Dome and Taylor Dome ice cores,
587 Antarctica: Sources and correlations. *J. Geophys. Res.* 108, 2374.

588 Fontijn, K., Lachowycz, S.M., Rawson, H., Pyle, D.M., Mather, T.A., Naranjo, J.A., Moreno-Roa, H., 2014. Late
589 Quaternary tephrostratigraphy of southern Chile and Argentina. *Quat Sci Rev* 89, 70-84.

590 Fujii, Y., Kohno, M., Motoyama, H., Matoba, S., Watanabe, O., Fujita, S., Azuma, N., Kikuchi, T., Fukuoka, T.,
591 Suzuki, T., 1999. Tephra layers in the Dome Fuji (Antarctica) deep ice core. *Annals of Glaciology*.

592 Geyer, A., Marti, A., Giralt, S., Folch, A., 2017. Potential ash impact from Antarctic volcanoes: Insights from
593 Deception Island's most recent eruption. *Sci Rep* 7, 16534.

594 Gutiérrez, F., Gioncada, A., González Ferran, O., Lahsen, A., Mazzuoli, R., 2005. The Hudson Volcano and
595 surrounding monogenetic centres (Chilean Patagonia): An example of volcanism associated with ridge-
596 trench collision environment. *J. Volcanol. Geoth. Res.* 145, 207-233.

597 Haberle, S.G., Lumley, S.H., 1998. Age and origin of tephra recorded in postglacial lake sediments to the
598 west of the southern Andes, 44°S to 47°S. *J. Volcanol. Geoth. Res.* 239-256, 239-256.

599 Haberzettl, T., Corbella, H., Fey, M., Janssen, S., Lücke, A., Mayr, C., Ohlendorf, C., Schäbitz, F., Schleser, G.H.,
600 Wille, M., Wulf, S., Zolitschka, B., 2007. Lateglacial and Holocene wet—dry cycles in southern Patagonia:
601 chronology, sedimentology and geochemistry of a lacustrine record from Laguna Potrok Aike, Argentina.
602 *The Holocene* 17, 297-310.

603 Harambour, S., 1988, Sobre el hallazgo del mitico volcan Reclus, ex Mano del Diablo, Hielo Patagonico Sur,
604 Magallanes, Chile. *Revista Geológica de Chile*. v. 15, 173-179.

605 Harpel, C.J., Kyle, P.R., Dunbar, N.W., 2008. Englacial tephrostratigraphy of Erebus volcano, Antarctica. *J.*
606 *Volcanol. Geoth. Res.* 177, 549-568.

607 Hole, M.J., Kempton, P.D., Millar, I.L., 1993. Trace-element and isotopic characteristics of small-degree melts
608 of the asthenosphere: evidence from the alkalic basalts of the Antarctic Peninsula. *Chem. Geol.* 109, 51-
609 68.

610 Houghton, B.F., Gonnermann, H.M., 2008. Basaltic explosive volcanism: Constraints from deposits and
611 models. *Chemie der Erde - Geochemistry* 68, 117-140.

612 Hubberten, H.-W., Wolfgang Morche, Westall, F., Fütterer, D.K., Keller, J., 1991. Geochemical investigations
613 of volcanic ash layers from southern Atlantic Legs 113 and 114. *Proceedings of the Ocean Drilling*
614 *Program, Scientific Results* 114, 733-749.

615 Kilian, R., Hohner, M., Biester, H., Wallrabe-Adams, H.J., Stern, C.R., 2003. Holocene peat and lake sediment
616 tephra record from the southernmost Chilean Andes (53-55°S). *Revista geológica de Chile* 30, 23-37.

617 Kliem, P., Enters, D., Hahn, A., Ohlendorf, C., Lisé-Pronovost, A., St-Onge, G., Wastegård, S., Zolitschka, B.,
618 2013. Lithology, radiocarbon chronology and sedimentological interpretation of the lacustrine record
619 from Laguna Potrok Aike, southern Patagonia. *Quat Sci Rev* 71, 54-69.

620 Kohno, M., Fujii, Y., Hirata, T., 2004. Chemical composition of volcanic glasses in visible tephra layers found
621 in a 2503 m deep ice core from Dome Fuji, Antarctica. *Annals of Glaciology* 39, 576-584.

622 Kratzmann, D., Carey, S., Scasso, R., Naranjo, J.-A., 2010. Role of cryptic amphibole crystallization in magma
623 differentiation at Hudson volcano, Southern Volcanic Zone, Chile. *Contrib. Mineral. Petrol.* 159, 237-
624 264.

625 Kraus, S., Kurbatov, A., Yates, M., 2013. Geochemical signatures of tephra from Quaternary Antarctic
626 Peninsula volcanoes. *Andean Geology* 40.

627 Kurbatov, A.V., Zielinski, G.A., Dunbar, N.W., Mayewski, P.A., Meyerson, E.A., Sneed, S.B., Taylor, K.C., 2006.
628 A 12,000 year record of explosive volcanism in the Siple Dome Ice Core, West Antarctica. *J. Geophys.*
629 *Res.* 111, D12307.

630 Le Bas, M.J., Le Maitre, R.W., Streckeisen, A., Zanettin, B., 1986. A chemical classification of volcanic rocks
631 based on the total alkali - silica diagram. *J. Petrol.* 27, 745-750.

632 Lowe, D., Alloway, B., 2015. Tephrochronology, in: Rink, W., Thompson, J. (Eds.), *Encyclopaedia of Scientific*
633 *Dating Methods*. Springer Dordrecht, pp. 783-799.

634 Lowe, D.J., 2011. Tephrochronology and its application: A review. *Quaternary Geochronology* 6, 107-153.

635 Martin, A., Cooper, A., Dunlap, W., 2010. Geochronology of Mount Morning, Antarctica: two-phase evolution
636 of a long-lived trachyte-basanite-phonolite eruptive center. *Bull. Volc.* 72, 357-371.

637 Martin, A.P., 2009. Mt. Morning, Antarctica: Geochemistry, geochronology, petrology, volcanology, and
638 oxygen fugacity of the rifted Antarctic lithosphere. University of Otago, Dunedin.

639 McCulloch, R.D., Bentley, M.J., 1998. Late glacial ice advances in the Strait of Magellan, southern Chile. *Quat*
640 *Sci Rev* 17, 775-787.

641 McCulloch, R.D., Davies, S.J., 2001. Late-glacial and Holocene palaeoenvironmental change in the central
642 Strait of Magellan, southern Patagonia. *Palaeogeogr. Palaeoclim. Palaeoecol.* 173, 143-173.

643 McCulloch, R.D., Fogwill, C.J., Sugden, D.E., Bentley, M.J., Kubik, P.W., 2005. Chronology of the last glaciation
644 in central strait of magellan and bahía inútil, southernmost south america. *Geografiska Annaler: Series*
645 *A, Physical Geography* 87, 289-312.

646 McDonough, W.F., Sun, S.-S., 1995. The composition of the Earth. *Chem. Geol.* 120, 223-253.

647 Moy, C.M., Dunbar, R.B., Moreno, P.I., Francois, J.-P., Villa-Martínez, R., Mucciarone, D.M., Guilderson, T.P.,
648 Garreaud, R.D., 2008. Isotopic evidence for hydrologic change related to the westerlies in SW Patagonia,
649 Chile, during the last millennium. *Quat Sci Rev* 27, 1335-1349.

650 Naranjo, J.A., Stern, C.A., 1998. Holocene explosive activity of Hudson Volcano, southern Andes. *Bull. Volc.*
651 59, 291-306.

652 Narcisi, B., Petit, J.R., Delmonte, B., 2010. Extended East Antarctic ice-core tephrostratigraphy. *Quat Sci Rev*
653 29, 21-27.

654 Narcisi, B., Petit, J.R., Delmonte, B., Basile-Doelsch, I., Maggi, V., 2005. Characteristics and sources of tephra
655 layers in the EPICA-Dome C ice record (East Antarctica): Implications for past atmospheric circulation
656 and ice core stratigraphic correlations. *Earth Planet. Sci. Lett.* 239, 253-265,
657 doi:210.1016/j.epsl.2005.1009.1005.

658 Narcisi, B., Petit, J.R., Delmonte, B., Scarchilli, C., Stenni, B., 2012. A 16,000-yr tephra framework for the
659 Antarctic ice sheet: a contribution from the new Talos Dome core. *Quat Sci Rev* 49, 52-63.

660 Narcisi, B., Petit, J.R., Langone, A., 2017. Last glacial tephra layers in the Talos Dome ice core (peripheral East
661 Antarctic Plateau), with implications for chronostratigraphic correlations and regional volcanic history.
662 *Quat Sci Rev* 165, 111-126.

663 Narcisi, B., Proposito, M., Frezzotti, M., 2001. Ice record of a 13th century explosive volcanic eruption in
664 northern Victoria Land, East Antarctica. *Ant. Sci.* 13, 174-181.

665 Nyland, R.E., Panter, K.S., Rocchi, S., Di Vincenzo, G., Del Carlo, P., Tiepolo, M., Field, B., 2013. Volcanic
666 activity and its link to glaciation cycles: single-grain age and geochemistry of Early Miocene volcanic
667 glass from ANDRILL AND-2A core, Antarctica. *J. Volcanol. Geoth. Res.* 250, 106-128.

668 Pearce, J.A., Hastie, A.R., Leat, P.T., Dalziel, I.W., Lawver, L.A., Barker, P.F., Millar, I.L., Barry, T.L., Bevins, R.E.,
669 2014. Composition and evolution of the Ancestral South Sandwich Arc: Implications for the flow of deep
670 ocean water and mantle through the Drake Passage Gateway. *Global and Planetary Change* 123, 298-
671 322.

672 Pearce, N., Westgate, J., Perkins, W., Preece, S., 2004. The application of ICP-MS methods to
673 tephrochronological problems. *Applied Geochemistry* 19, 289-322.

674 Pearce, N.J.G., Perkins, W.T., Westgate, J.A., Gorton, M.P., Jackson, S.E., Neal, C.R., Chenery, S.P., 1997. A
675 compilation of new and published major and trace element data for NIST SRM 610 and NIST SRM 612
676 glass reference materials. *Geostandards and Geoanalytical Research* 21, 115-144.

677 Pérez, W., Freundt, A., Kutterolf, S., Schmincke, H.U., 2009. The Masaya Triple Layer: A 2100 year old basaltic
678 multi-episodic Plinian eruption from the Masaya Caldera Complex (Nicaragua). *J. Volcanol. Geoth. Res.*
679 179, 191-205.

680 Petrelli, M., Laeger, K., Perugini, D., 2016a. High spatial resolution trace element determination of geological
681 samples by laser ablation quadrupole plasma mass spectrometry: implications for glass analysis in
682 volcanic products. *Geosciences Journal*, 1-21.

683 Petrelli, M., Morgavi, D., Vetere, F., Perugini, D., 2016b. Elemental imaging and petro-volcanological
684 applications of an improved laser ablation inductively coupled quadrupole plasma mass spectrometry.
685 *Per. Mineral.* 85, 25-39.

686 Petrelli, M., Perugini, D., Alagna, K.E., Poli, G., Peccerillo, A., 2008. Spatially resolved and bulk trace element
687 analysis by laser ablation - inductively coupled plasma - mass spectrometry (LA-ICP-MS). *Per. Mineral.*
688 77, 3-21.

689 Prieto, A., Stern, C.R., Estévez, J.E., 2013. The peopling of the Fuego-Patagonian fjords by littoral hunter-
690 gatherers after the mid-Holocene H1 eruption of Hudson Volcano. *Quaternary International* 317, 3-13.

691 Puig, A., Herve, M., Suarez, M., Saunders, A.D., 1984. Calc-alkaline and alkaline Miocene and calc-alkaline
692 recent volcanism in the southernmost Patagonian Cordillera, Chile. *J. Volcanol. Geotherm. Res.*, 21, 149-
693 163.

694 Reimer, P.J., Bard, E., Bayliss, A., Beck, J.W., Blackwell, P.G., Ramsey, C.B., Buck, C.E., Cheng, H., Edwards,
695 R.L., Friedrich, M., Grootes, P.M., Guilderson, T.P., Haflidason, H., Hajdas, I., Hatté, C., Heaton, T.J.,
696 Hoffmann, D.L., Hogg, A.G., Hughen, K.A., Kaiser, K.F., Kromer, B., Manning, S.W., Niu, M., Reimer, R.W.,
697 Richards, D.A., Scott, E.M., Southon, J.R., Staff, R.A., Turney, C.S.M., van der Plicht, J., 2013. IntCal13 and
698 Marine13 Radiocarbon Age Calibration Curves 0–50,000 Years cal BP. *Radiocarbon* 55, 1869-1887.

699 Scasso, R.A., Corbella, H., Tiberi, P., 1994. Sedimentological analysis of the tephra from the 12–15 August
700 1991 eruption of Hudson volcano. *Bull. Volc.* 56, 121-132.

701 Shane, P., Nairn, I.A., Martin, S.B., Smith, V.C., 2008. Compositional heterogeneity in tephra deposits
702 resulting from the eruption of multiple magma bodies: Implications for tephrochronology. *Quaternary*
703 *International* 178, 44-53.

704 Stern, C., 2004. Active Andean Volcanism: its geologic and tectonic setting. *Revista Geologica Chile* 31, 161-
705 206.

706 Stern, C., Futa, K., Muehlenbachs, K., 1984. Isotope and trace element data for orogenic andesites from the
707 austral Andes, in: Harmon, R., Barreiro, B.A. (Eds.), *Andean Magmatism: Chemical and Isotopic*
708 *Constraints*. Shiva.

709 Stern, C.H., 1991. Mid-Holocene tephra on Tierra del Fuego (54°S) derived from the Hudson volcano (46°S):
710 evidence for a large explosive eruption. *Revista Geologica de Chile* 18, 139-146.

711 Stern, C.R., 2008. Holocene tephrochronology record of large explosive eruptions in the southernmost
712 Patagonian Andes. *Bull. Volc.* 70, 435-454.

713 Stern, C.R., Kilian, R., 1996. Role of the subducted slab, mantle wedge and continental crust in the
714 generation of adakites from the Andean Austral Volcanic Zone. *Contrib. Mineral. Petrol.* 123, 263-281.

715 Stern, C.R., Moreno, P.I., Villa-Martínez, R., Sagredo, E.A., Prieto, A., Labarca, R., 2011. Evolution of ice-
716 dammed proglacial lakes in Última Esperanza, Chile: implications from the late-glacial R1 eruption of
717 Reclús volcano, Andean Austral Volcanic Zone. *Andean Geology* 38, 82-97.

718 Stuiver, M., Reimer, P.J., and Reimer, R.W., 2018, CALIB 7.1 [WWW program] at <http://calib.org>, accessed
719 2018-7-10

720 Villa-Martínez, R., Moreno, P.I., 2007. Pollen evidence for variations in the southern margin of the westerly
721 winds in SW Patagonia over the last 12,600 years. *Quaternary Research* 68.

722 Wastegård, S., Veres, D., Kliem, P., Hahn, A., Ohlendorf, C., Zolitschka, B., 2013. Towards a late Quaternary
723 tephrochronological framework for the southernmost part of South America – the Laguna Potrok Aike
724 tephra record. *Quat Sci Rev* 71, 81-90.

725 Watt, S.F.L., Pyle, D.M., Mather, T.A., 2013. The volcanic response to deglaciation: Evidence from glaciated
726 arcs and a reassessment of global eruption records. *Earth-Science Reviews* 122, 77-102.

- 727 Weller, D., Miranda, C.G., & P.I.M., Villa-Martínez, R., Stern, C.R., 2014. The large late-glacial Ho eruption of
728 the Hudson volcano, southern Chile. *Bull. Volc.* 76, 831.
- 729 Weller, D.J., Miranda, C.G., Moreno, P.I., Villa-Martínez, R., Stern, C.R., 2015. Tephrochronology of the
730 southernmost Andean Southern Volcanic Zone, Chile. *Bull. Volc.* 77, 1-24.
- 731 Wilch, T.I., McIntosh, W.C., Dunbar, N.W., 1999. Late Quaternary volcanic activity in Marie Byrd Land:
732 Potential $^{40}\text{Ar}/^{39}\text{Ar}$ -dated time horizons in Westa Antarctic ice and marine cores. *Geol. Soc. Am. Bull.*
733 111, 1563-1580.
- 734

735 **Table captions**

736 Table 1 Synoptic scheme of the features of studied tephra layers.

737 Table 2 Major and trace element compositions of glass in studied samples.

738 Table 3 Radiocarbon age results.

739

740 **Figure captions**

741 Figure 1 - Map of southernmost South America showing the locations of the Holocene volcanoes, the
742 extent of the Austral Volcanic Zone of the Andes, and the tephra outcrops studied in this work.

743 Abbreviations: AR, Arroyo Robles; RR, Río Rubens; EO, Estancia Otway; ROH, Río O'Higgins;

744 PA, Punta Arenas; LA, Laguna de los Cisnes; RTB, Río Tres Brazos. The inset shows the Southern

745 Hemisphere with the localities mentioned in the text: F, Dome Fuji; V, Vostok Station; C, Dome C;

746 T, Taylor Dome; A, Andrill; S, Siple Dome; W, WAIS Divide.

747

748 Figure 2 - Photographs of the studied stratigraphic sections. a: Estancia Otway 1; b: Estancia Otway

749 2; c: Punta Arenas; d: Río Tres Brazos 1; e: Río Tres Brazos 2; f: Laguna de los Cisnes; g: Río

750 O'Higgins; h: Arroyo Robles; i: Río Rubens.

751

752 Figure 3 - Logs of studied stratigraphic sections and their correlations.

753

754 Figure 4 - Scanning electron microscope back-scattered (SEM-BSE) images of tephra samples. a:

755 EO-1B tephra; b: EO-1C tephra; c: EO-2B tephra; d: EO-2D tephra; e: EO-2H tephra; f: EO-2I

756 tephra.

757

758 Figure 5 - Scanning electron microscope back-scattered (SEM-BSE) images of tephra samples. a:

759 PA-1B tephra; b: RTB-2B tephra; c: RTB-1B tephra; d: LA-1B tephra.

760

761 Figure 6 - Scanning electron microscope back-scattered (SEM-BSE) images of tephra samples. a:
762 ROH-2B tephra; b: ROH-2C tephra; c: AR-1B tephra; d: AR-1D tephra; e: AR-1F tephra; f: RR-2B
763 tephra.

764

765 Figure 7 - a: Total alkali vs Silica diagram (TAS) (Le Bas et al., 1986); b: K_2O versus SiO_2 diagram.

766

767 Figure 8 - Primordial mantle-normalized multi-element patterns (McDonough and Sun, 1995). a: all
768 studied samples; b: Group Tr samples; c: Group Rh1 samples; d: Group Rh2 samples.

769

770 Figure 9 - a: Nb/Ba vs La/Zr; b: Rb/Ba vs Ti/Sm; c: Rb/Ba vs Sr/Nd; d: Ce/Pb vs Ba/Th for the glass
771 shards of tephra layers studied in this work. Each data point represents a single LA-ICP-MS point
772 analysis.

773

774 Figure 10 - K_2O vs SiO_2 diagrams reporting literature data compared with data of this work in which
775 the volcanic sources are unambiguously distinguished; a: Hudson (Group Tr); b: Mt Burney (Group
776 Rh1); c: Reclus (Group Rh2).

777

778 Figure 11 - Selected trace element diagrams for comparison of volcanic sources with this work data.

779

780 Figure 12 - Volume and age of the major eruptions from Hudson, Mt Burney and Reclus (Watt et al.,
781 2013; Weller et al., 2015) in comparison with the age of eruptions here discussed. Red lines
782 represent intervals for eruption ages defined by two ^{14}C ages (Table 3), red arrows represent intervals
783 for eruption ages defined by only one ^{14}C ages bounding the possible oldest or youngest age (Table
784 3).

785

786 Figure 13 - K₂O vs SiO₂ plot comparing compositional groups of tephra collected in Antarctic, Peri-
787 Antarctic and South American regions. Antarctic tephra come from (i) englacial layers from Marie
788 Byrd Land (MBL) and northern Victoria Land (NVL) (Dunbar et al., 2008; Wilch et al., 1999),
789 <http://www.tephrochronology.org/AntT/about.html>, and East Antarctica (Curzio et al., 2008; Harpel
790 et al., 2008); in this group highly evolved samples of Lineage 1c are included (Martin et al., 2010;
791 Martin, 2009), (ii) ice cores drilled in Fuji Dome (Fujii et al., 1999; Kohno et al., 2004), Taylor
792 Dome (Dunbar et al., 2003), Siple Dome (Dunbar and Kurbatov, 2011; Kurbatov et al., 2006),
793 <http://www.tephrochronology.org/AntT/about.html>, West Antarctic Divide-WDC (Dunbar et al.,
794 2017), Vostok (Basile et al., 2001; Narcisi et al., 2010), Dome C (Narcisi et al., 2010; Narcisi et al.,
795 2005), Talos Dome (Narcisi et al., 2010; Narcisi et al., 2012; Narcisi et al., 2017; Narcisi et al., 2001)
796 and (iii) offshore ANDRILL deep cores (Del Carlo et al., 2009; Di Roberto et al., 2012; Nyland et
797 al., 2013) and gravity cores (Del Carlo et al., 2015). Peri-Antarctic tephra are from South Shetland
798 Islands (Hole et al., 1993; Kraus et al., 2013) and from marine tephra attributed to South Sandwich
799 sources (Hubberten et al., 1991). Tephra from South America are from semi-distal to distal layers
800 collected in Patagonia and Tierra del Fuego and attributed to an Andean sources, i.e. the volcanoes
801 Hudson (Gutiérrez et al., 2005; Kratzmann et al., 2010; Naranjo and Stern, 1998; Weller et al.,
802 2014), Reclus (Kilian et al., 2003; Stern and Kilian, 1996), Mt Burney (Kilian et al., 2003; Stern,
803 2008; Stern and Kilian, 1996), Aguilera (Kilian et al., 2003; Stern, 2008), Cook (Stern and Kilian,
804 1996), Macá and Cay (Gutiérrez et al., 2005), as well as from layer studied in this work. For
805 locations see Figure 1. Specific samples mentioned in the text are labeled (same color as symbol).

806

807 **Supplementary Material Table 1**

808 Dataset of major and trace elements data and secondary standard analyses.

809

810

811 **Supplementary Material Table 2**

812 Major- and trace-element data for tephra from Antarctic ice cores, marine sediments, blue ice,
813 continental outcrops as well as for potential sources located in Antarctica and circum-Antarctic areas.
814

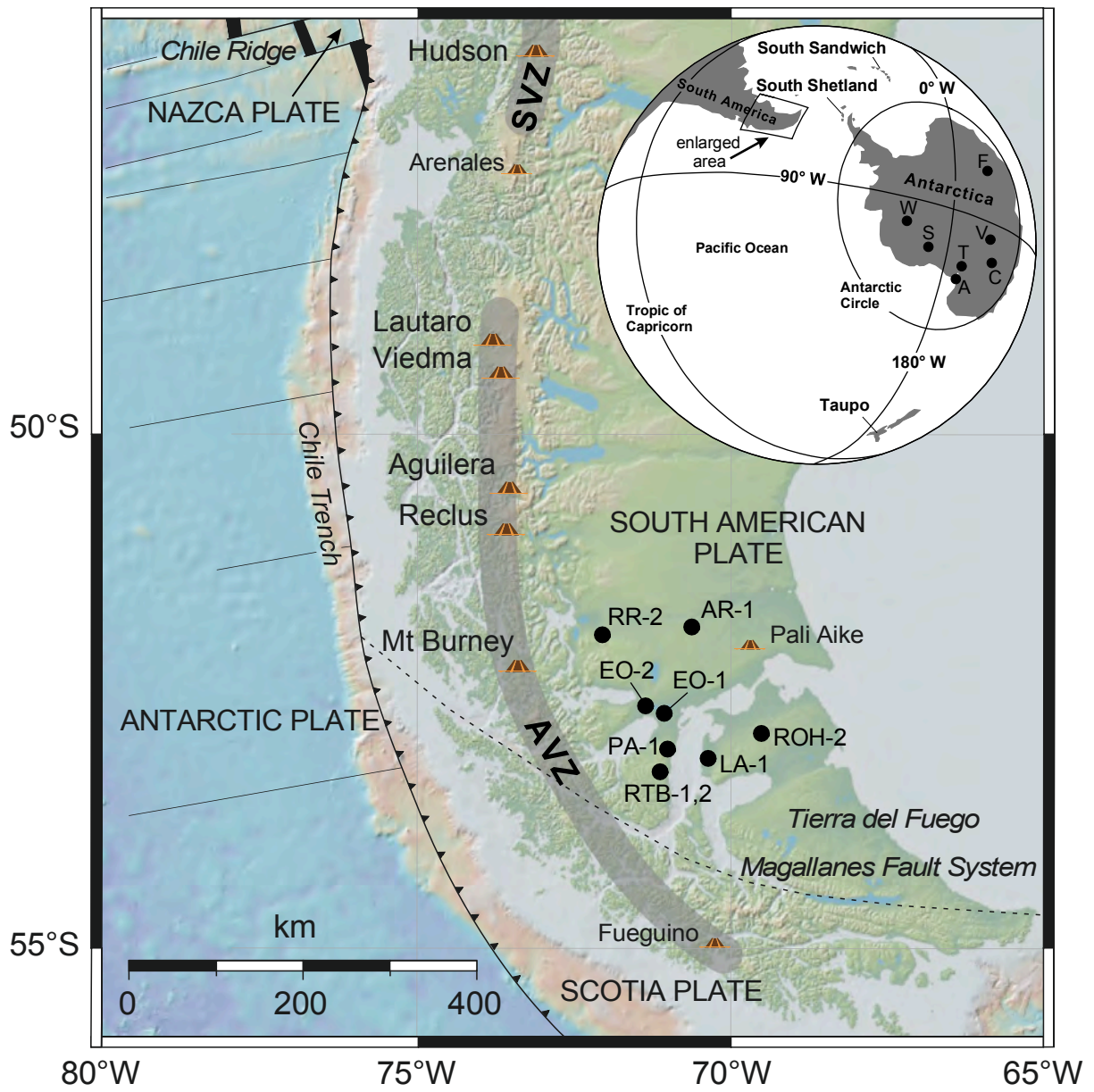
Section	PA-1	RTB-1	RTB-2	LA-1	EO-1	EO-2	ROH-2	AR-1	RR-2								
Lat. S	53°10'14.9"	53°17'23.70"	53°17'25.26"	53°14'43.20"	52°47'28.58"	52°44'44.64"	52°56'12.60"	51°51'27.77"	52°33'7.14"								
Long. W	070°56'19.3"	71°1'12.60"	71°1'12.66"	70°18'58.74"	71°5'19.41"	71°20'58.98"	69°25'48.00"	70°25'37.54"	71°59'24.78"								
Sample	PA-1B	RTB-1B	RTB-2B	LA-1B	EO-1B	EO-2B	ROH-2B	AR-1B	RR-2B								
Thickness (cm)	2-5	12-15	1-3	3-7, discontinuous	1-3	2-4	2	2	2								
Color	grey-white (Fig. 2c)	white-grey (Fig. 2d)	white (Fig. 2d)	grey (Fig. 2f)	grey (Fig. 2a)	pale yellow (Fig. 2b)	milky white (Fig. 2b)	honey (Fig. 2b)	grey (Fig. 2b)	grey (Fig. 2b)	pale white (Fig. 2g)	pale yellow (Fig. 2g)	white (Fig. 2h)	pale grey (Fig. 2h)	pale yellow (Fig. 2h)	grey-white (Fig. 2i)	
Grain size	very fine	fine	very fine	very fine	very fine	fine	very fine	fine to coarse ash	very fine	very fine	fine	very fine	fine to coarse ash	fine to coarse ash	very fine	fine to coarse ash	
Glass shards	blocky, Y-shaped and cusate glass shards, bubble walls and bubble junctions; size from few µm up to ~100 µm (Fig. 5a)	<20 µm blocky to y-shaped or cusate glass shards (Fig. 5c)	<20 µm, bubble junctions and y-shaped glass shards; poorly-vesicular blocky glass fragments <100 µm with spherical to ellipsoidal and coalesced vesicles	<50 µm, moderately- to poorly-vesicular, blocky glass particles and y-shaped, bubble walls and junctions (Fig. 5d); with scarce pl, opx, ap	minor <100 µm micropumices occur with tubular, vesicular and occasional microlites of pl, opx, Fe-Ti ox, ap	few micropumices with tubular vesicles and occasional microlites of pl, opx, Fe-Ti ox, ap	few moderately to highly-vesicular micropumices	abundant ~100 µm to 1 mm, highly-vesicular micropumices with coalesced and collapsed vesicles. Some of the micropumices show microlite-rich groundmass	minor, <2 mm, highly- to moderately-vesicular micropumices with coalesced and collapsed vesicles, bearing microcrystals of pl, qz, opx, Fe-Ti spinels, cpx and ap (Fig. 4d).	abundant loose crystals of pl, qz, opx, Fe-Ti spinels, cpx and ap coated with vesicular to dense glass	scarce loose crystals of pl, opx, cpx and ap	abundant loose crystals of pl, qz, opx, Fe-Ti spinels and ap coated with volcanic glass and few µm blocky glass shards, bubble walls and bubble junctions (Fig. 4f)	loose crystals of pl, opx, cpx, qz and apatite	<500 µm, loose crystals of pl, qz, opx, Fe-Ti spinels, cpx and ap coated with vesicular glass	<500 µm, loose crystals of pl, qz, opx, Fe-Ti spinels, cpx and ap coated with moderately vesicular glass	loose crystals of cpx, pl and opx with elongated, collapsed vesicles	<2 mm, loose crystals of pl, opx, cpx, qz often coated with moderately vesicular glass (Fig. 6f); crystals with cracks and alteration textures along the cracks
Micropumices	some highly vesicular and almost aphyric micropumices, <300 µm in size with coalesced and collapsed vesicles	moderately- to highly-vesicular micropumices <200 µm	minor highly- to moderately-vesicular micropumices <200 µm (Fig. 5b); micropumices with microlites of pl, opx, cpx, Fe-Ti ox, ap	minor <100 µm micropumices occur with tubular, vesicular and occasional microlites of pl, opx, Fe-Ti ox, ap	few micropumices with tubular vesicles and occasional microlites of pl, opx, Fe-Ti ox, ap	few moderately to highly-vesicular micropumices	abundant ~100 µm to 1 mm, highly-vesicular micropumices with coalesced and collapsed vesicles. Some of the micropumices show microlite-rich groundmass	minor, <2 mm, highly- to moderately-vesicular micropumices with coalesced and collapsed vesicles, bearing microcrystals of pl, qz, opx, Fe-Ti spinels, cpx and ap (Fig. 4d).	abundant loose crystals of pl, qz, opx, Fe-Ti spinels and ap coated with vesicular to dense glass	scarce loose crystals of pl, opx, cpx and ap	abundant loose crystals of pl, qz, opx, Fe-Ti spinels and ap coated with volcanic glass and few µm blocky glass shards, bubble walls and bubble junctions (Fig. 4f)	loose crystals of pl, opx, cpx, qz and apatite	<500 µm, loose crystals of pl, qz, opx, Fe-Ti spinels, cpx and ap coated with vesicular glass	<500 µm, loose crystals of pl, qz, opx, Fe-Ti spinels, cpx and ap coated with moderately vesicular glass	loose crystals of cpx, pl and opx with elongated, collapsed vesicles	<2 mm, loose crystals of pl, opx, cpx, qz often coated with moderately vesicular glass (Fig. 6f); crystals with cracks and alteration textures along the cracks	
Crystals	loose crystals of cpx, opx, pl and Fe-Ti ox often coated with vesicular glass	loose crystals of pl, opx, cpx, Fe-Ti ox, ap, wetted by vesicular volcanic glass	loose crystals of pl, opx, cpx, Fe-Ti oxides, ap, wetted by vesicular volcanic glass	scarce loose crystals of pl, opx, ap	scarce loose crystals of pl <150 µm	<200 µm, loose euhedral to subhedral crystals of pl, opx, cpx, ap, Fe-Ti oxides coated with highly-vesicular glass; crystals with cracks and perforation patterns (channels or tunnels)	present	present	present	well-rounded lithic fragments of holocrystalline volcanic rocks	rare fragments of holocrystalline rocks	holocrystalline volcanic rocks	holocrystalline volcanic rocks	holocrystalline rock fragments are scarce	tephra topped by a soil layer rich in organic matter with dispersed charcoals has been observed (sample RR-2A; Fig. 2i)		
Lithics	well rounded volcanic rock grains and abundant diatoms	abundant fragments and crystals with cracks and perforation patterns (channels or tunnels)	volcanic rock grains	scarce holocrystalline volcanic rock fragments													
Stratigraphic notes	layer sandwiched between two soils (PA-1C, above and PA-1A, below), with desiccation cracks (Fig. 2c)	top and bottom of the layer slightly reworked and diffuse; charcoal fragments (sample RTB-1C) dispersed in the uppermost 3 cm of the tephra	deposited over a cm-thick peat layer (sample RTB-2A), resting on the top of a metres-thick conglomerate (Fig. 2e)	tephra lies on a dark brown soil several cm-thick (sample LA-1A; Fig. 2f)	emplaced over a peat layer (Fig. 2a)	emplaced over a peat layer (Fig. 2a)	layer interbedded with peat layer (Fig. 2b)	layer interbedded with peat layer (Fig. 2b)				lowest layers, lying with wavy basal contact over a peat layer several cm-thick (sample ROH-2A; Fig. 2g)		lowest layer in the section; embedded between two peat layers (samples AR-1A, AR-1C, Fig. 2h)	mid layer in the section; sandwiched between two peat layers (samples AR-1C, AR-1E, Fig. 2h)	uppermost layer in the section (Fig. 2h)	tephra topped by a soil layer rich in organic matter with dispersed charcoals has been observed (sample RR-2A; Fig. 2i)

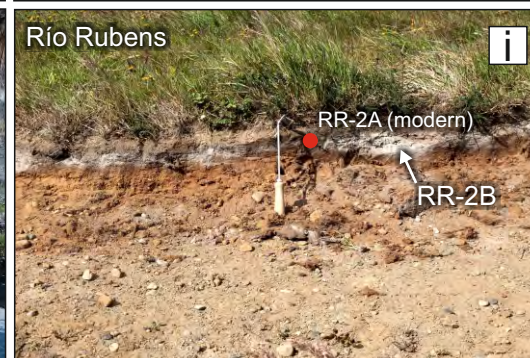
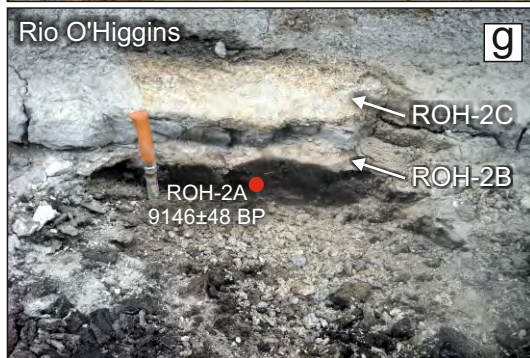
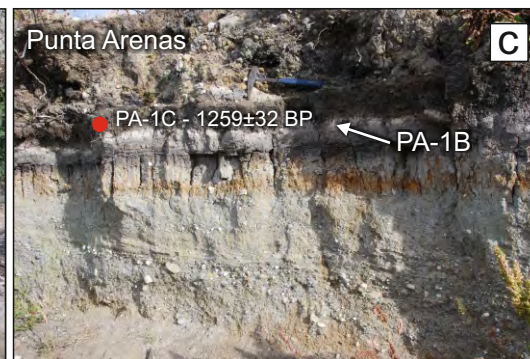
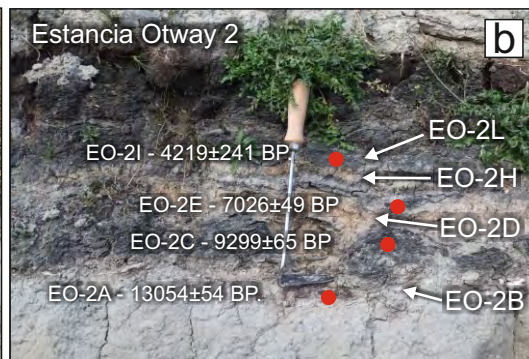
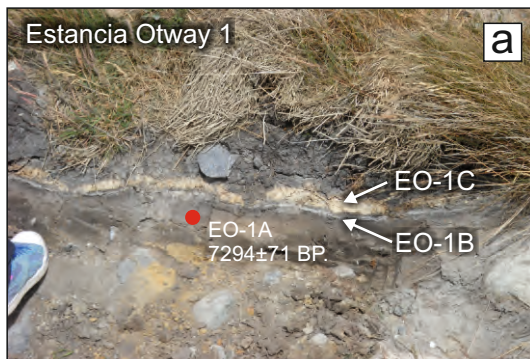
Abbreviations: cpx, clinopyroxene; opx, orthopyroxene; pl, plagioclase; ox, oxides; ap, apatite

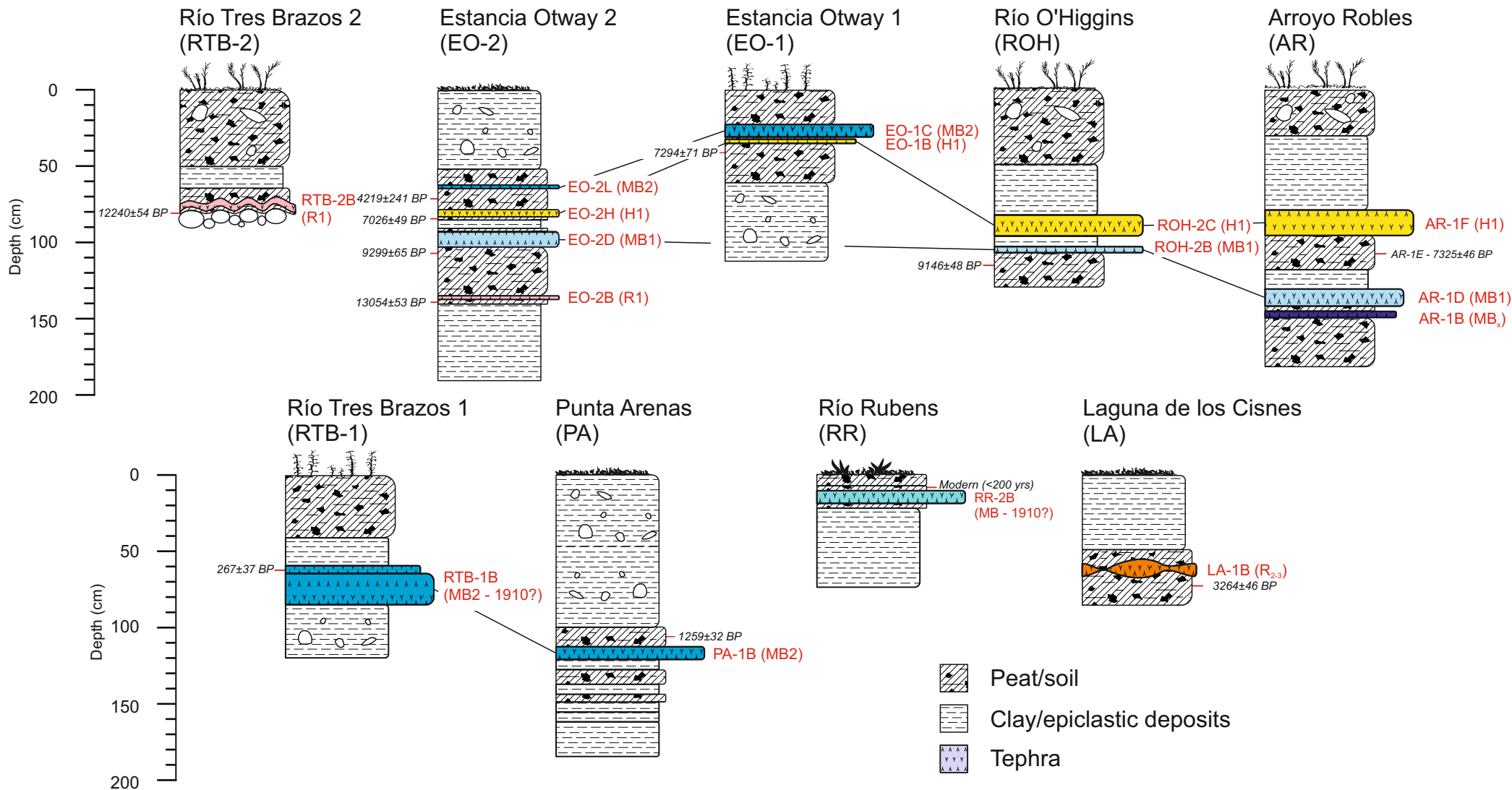
Table 3. Radiocarbon age results

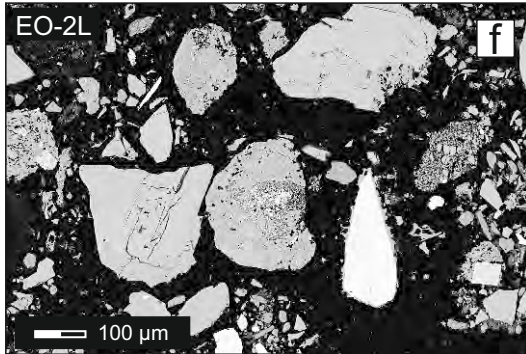
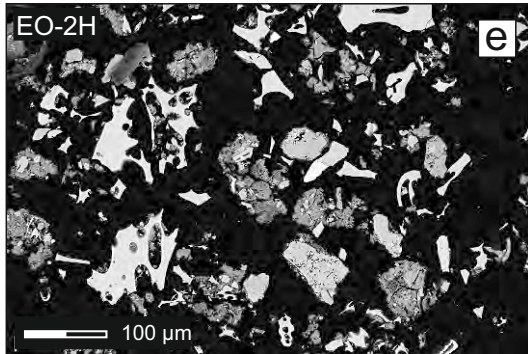
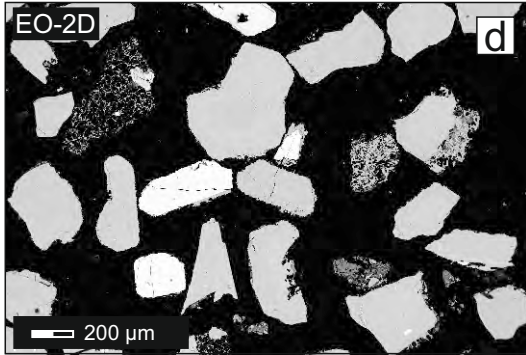
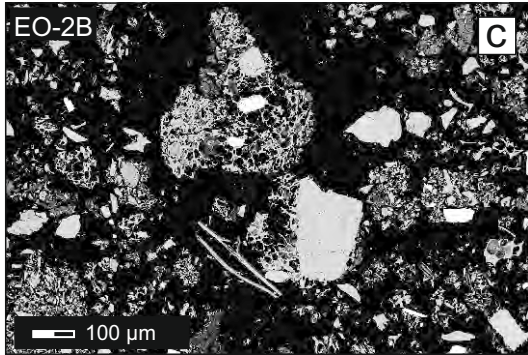
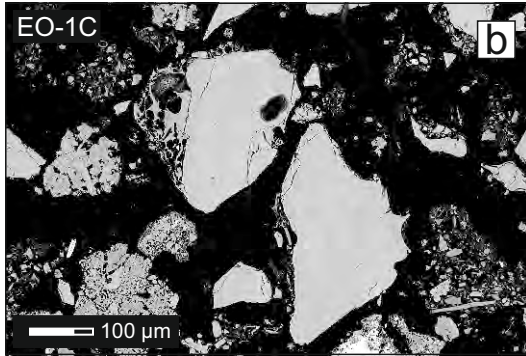
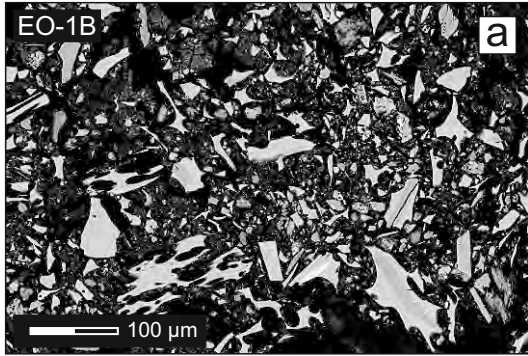
Sample Label	Laboratory code	Material	¹⁴ C yrs BP	¹⁴ C cal yrs BP (range 2σ)	median cal year BP	δ ¹³ C‰ V- PDB
RTB-1C	RC479	Charcoal	267±37	277-459	321	-38.13±1.43
RTB-2A	RC491	SOM	12240±54	13966-14402	14143	-26.54±2.04
PA-1C	RC475	Charcoal	1259±32	1084-1281	1216	-14.07±0.80
LA-1A	RC494	SOM	3264±46	3385-3585	3495	-24.78±4.40
EO-1A	RC486	SOM	7294±71	7965-8303	8106	-37.29±1.25
EO-2I	RC490	SOM	4219±241	4090-5461	4762	-29.60±0.84
EO-2C	RC488	SOM	9299±65	10276-10661	10490	-24.12±4.63
EO-2E	RC489	SOM	7026±49	7744-7955	7865	-36.02±1.35
EO-2A	RC477	Charcoal	13054±54	15359-15861	15643	-30.77±1.26
ROH-2A	RC493	SOM	9146±48	10224-10482	10308	-33.42±1.73
AR-1E	RC485	SOM	7325±46	8014-8291	8119	-22.32±1.68
RR-2A	RC481	SOM	9±38	Modern	Modern	-24.39±4.54

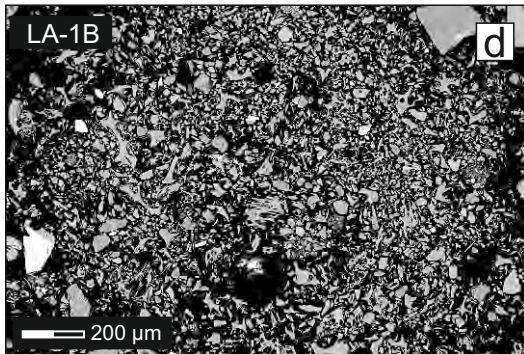
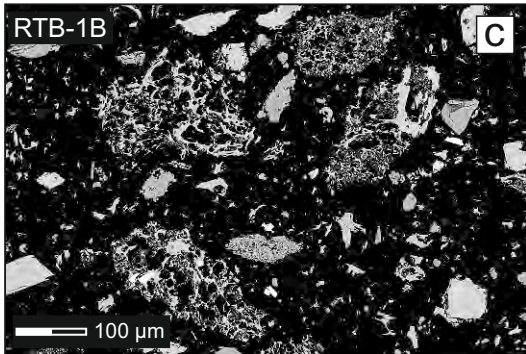
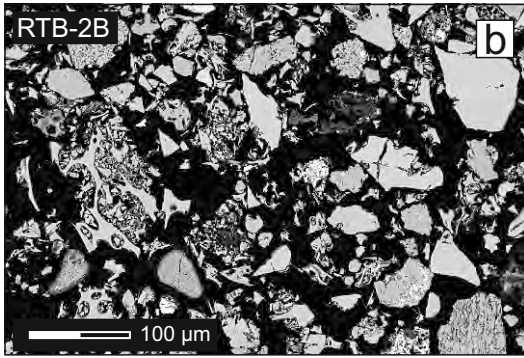
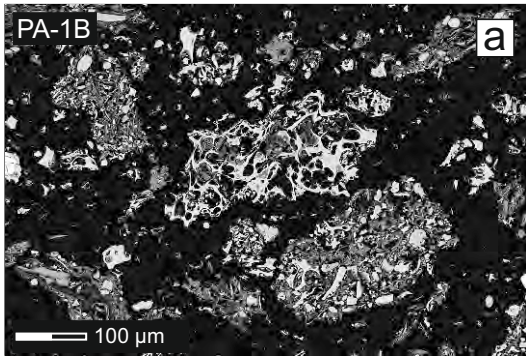
Abbreviations: SOM, soil organic matter

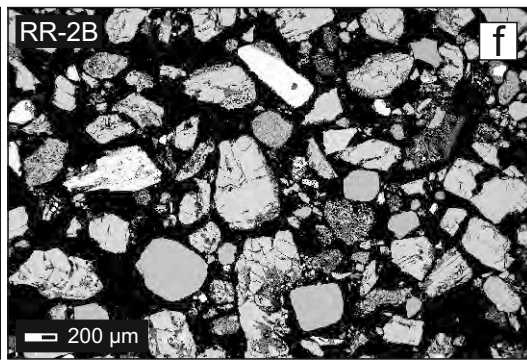
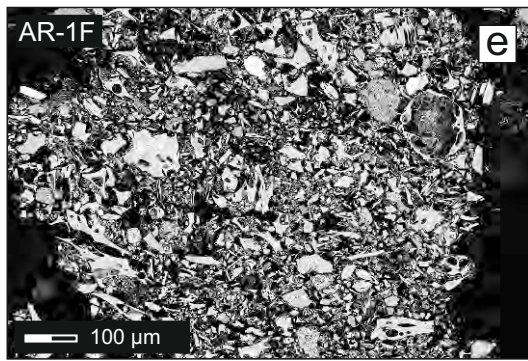
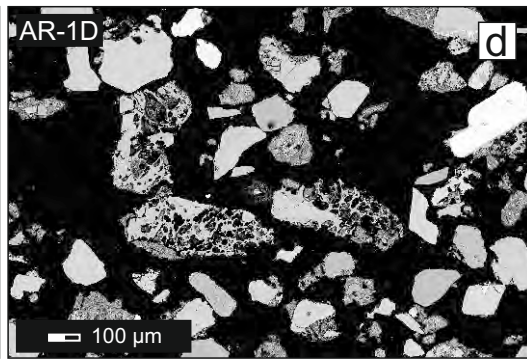
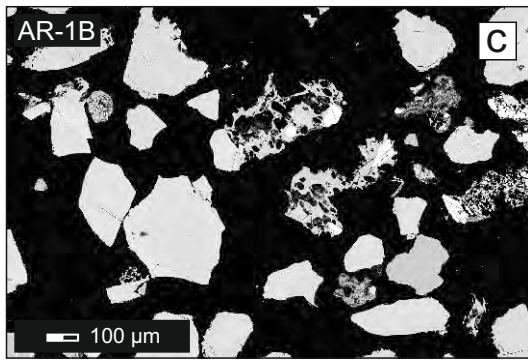
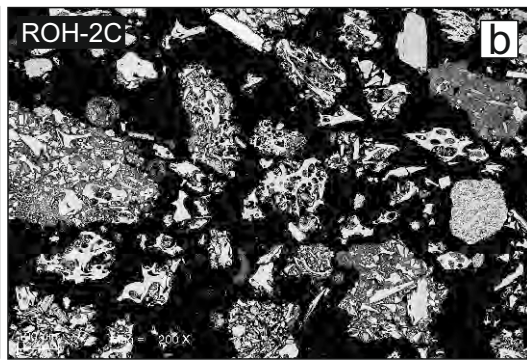
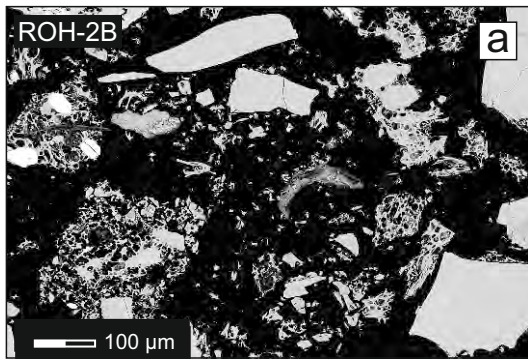


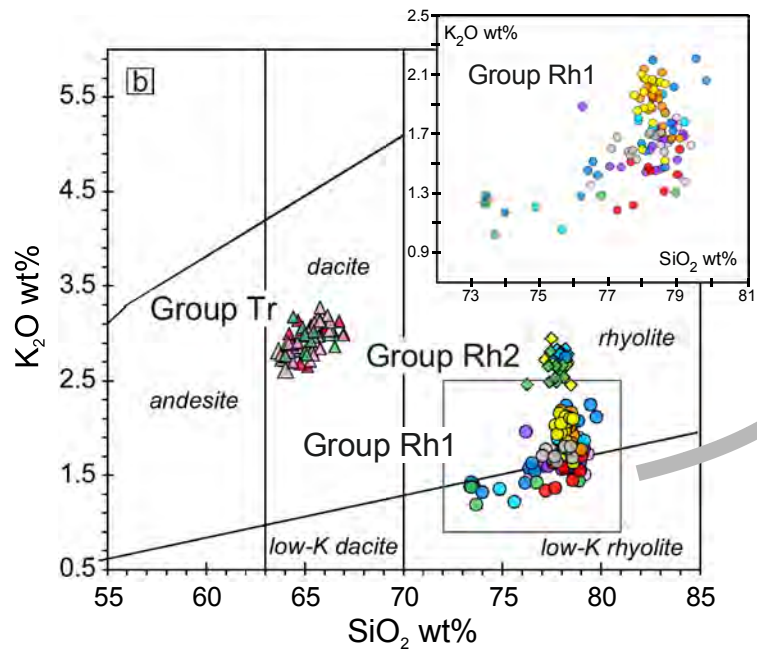
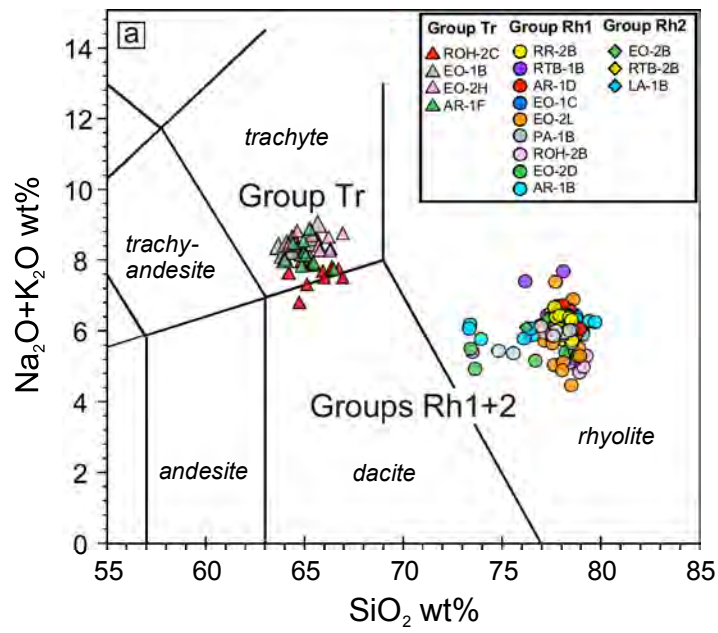


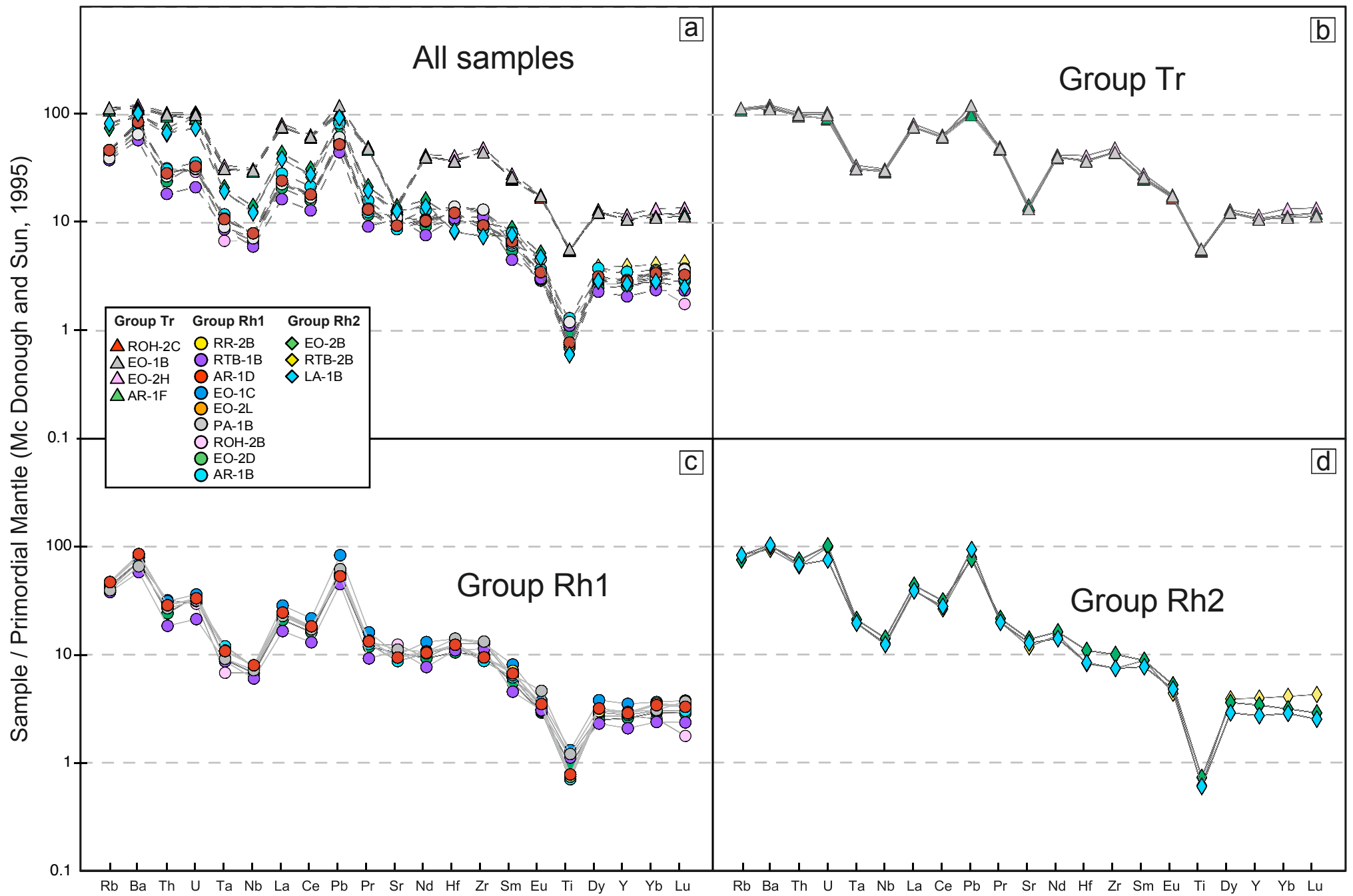


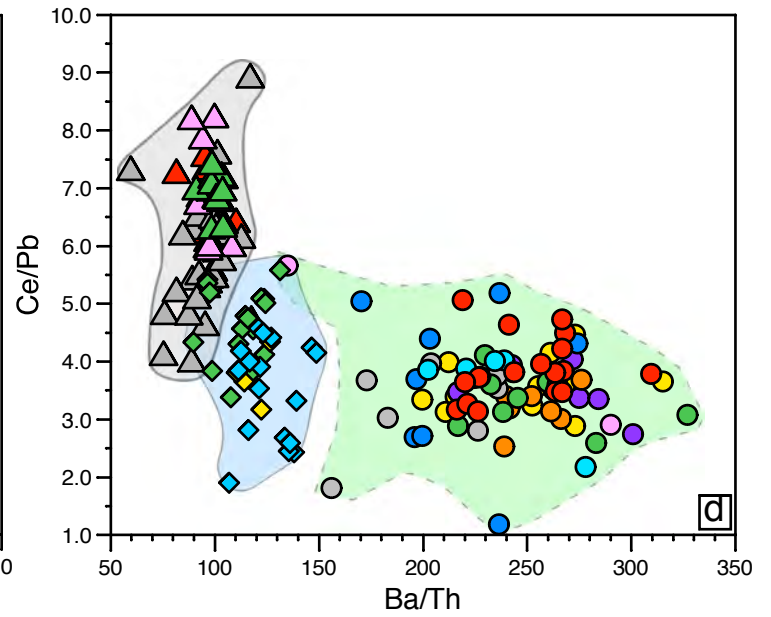
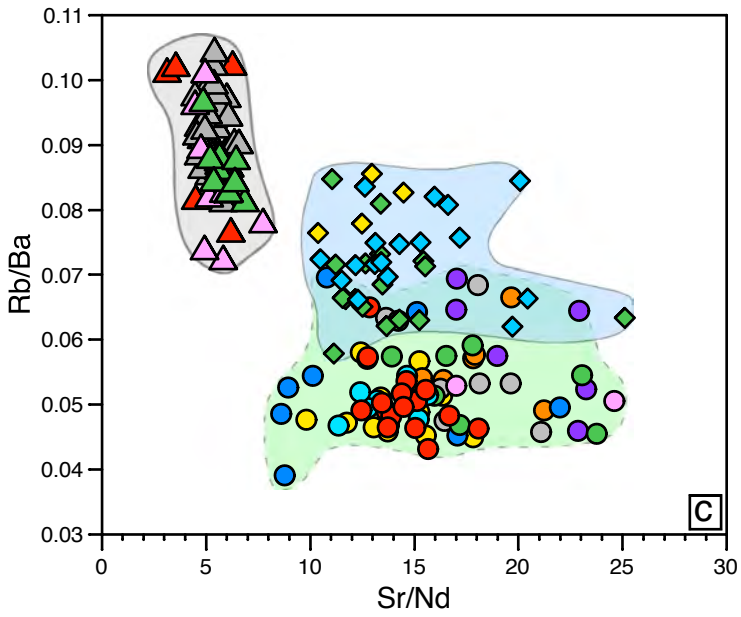
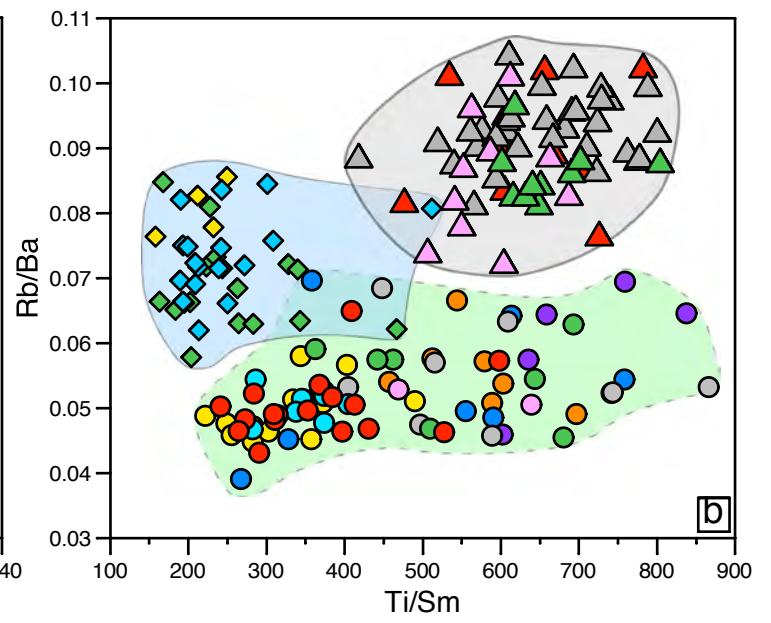
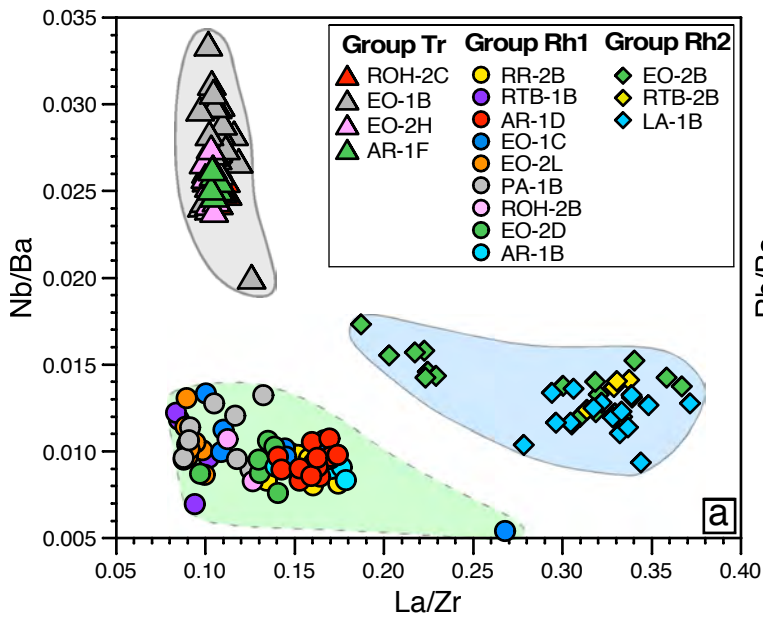


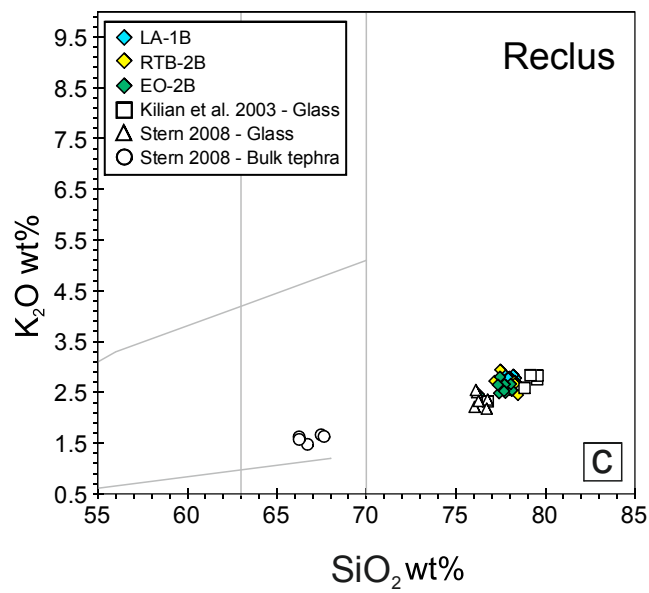
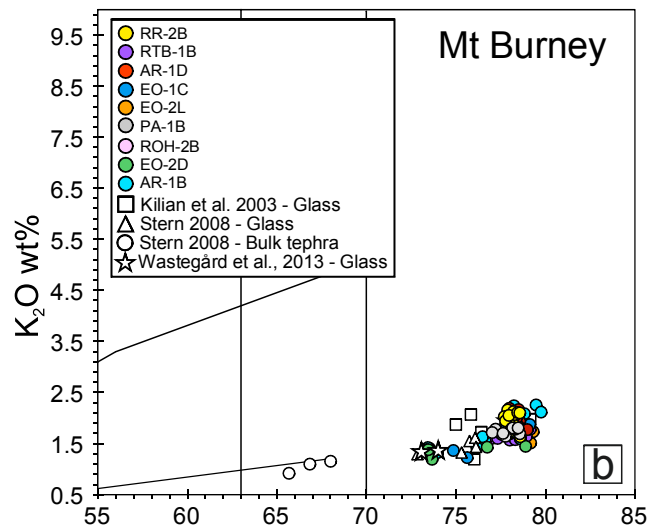
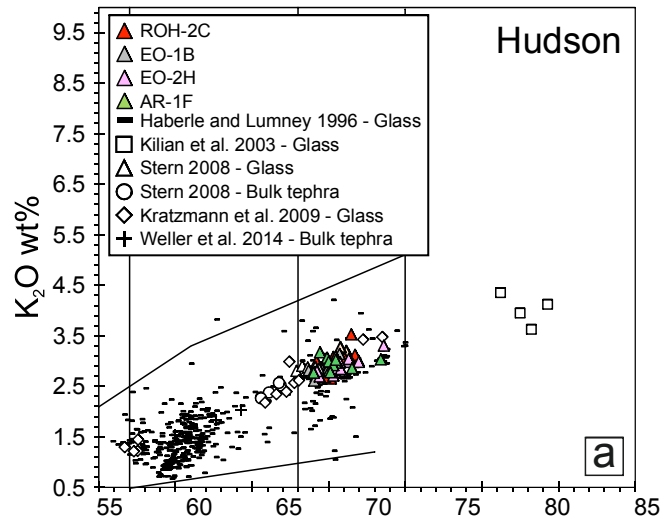






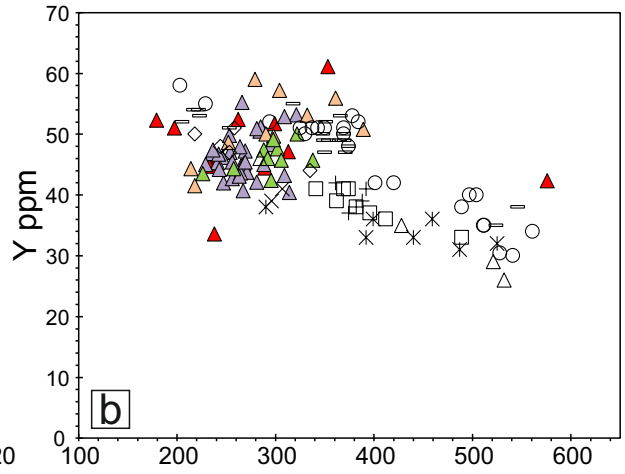
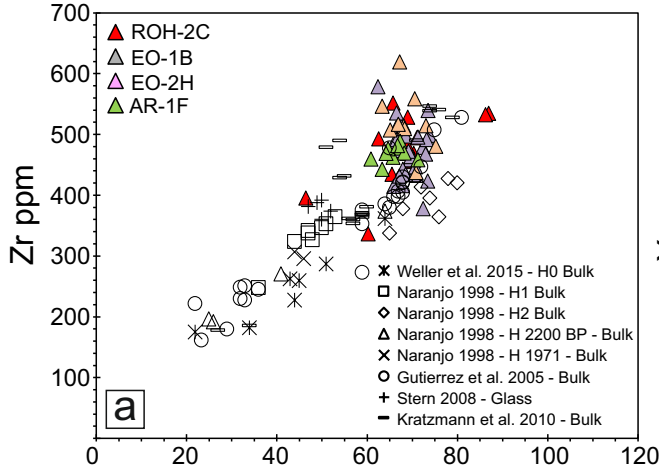




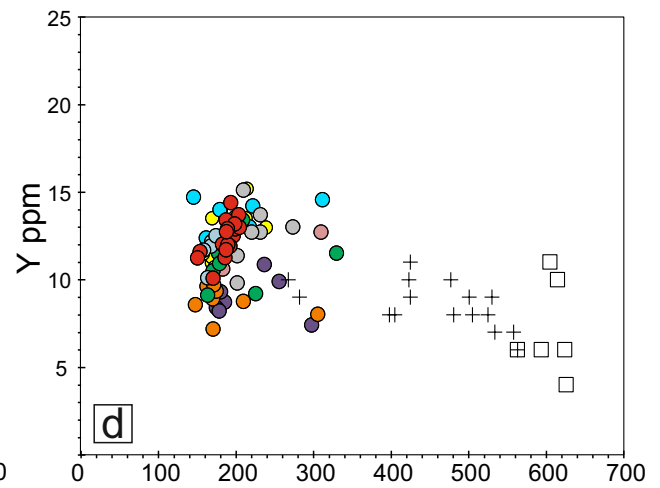
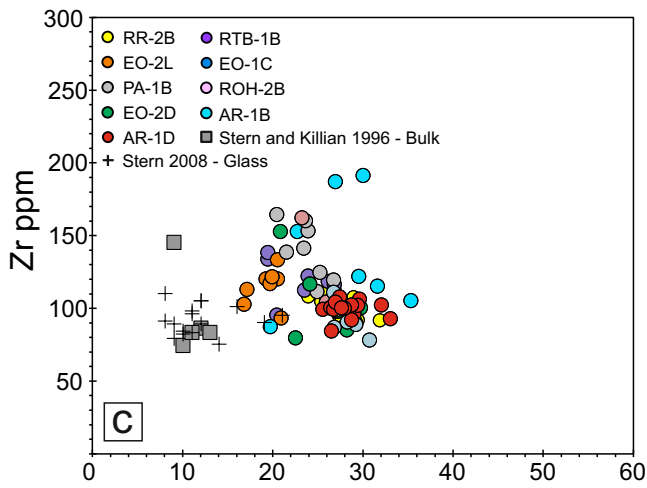


SiO_2 wt%

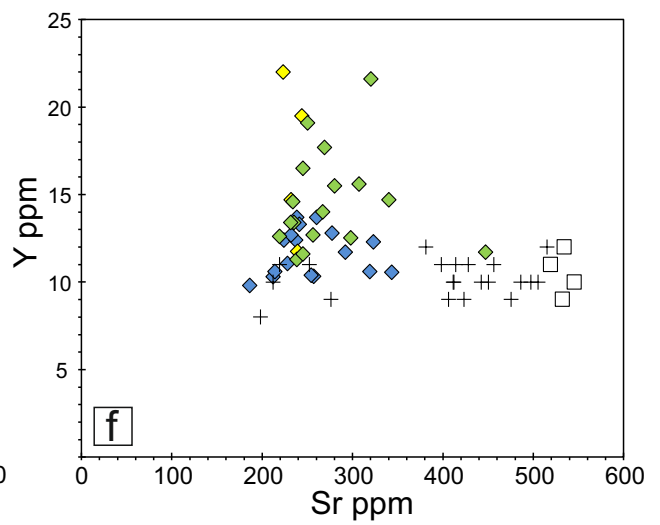
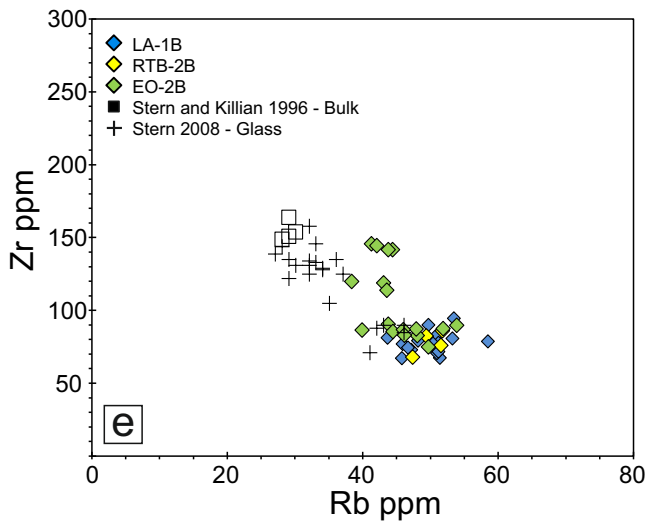
Hudson

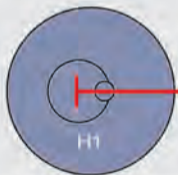
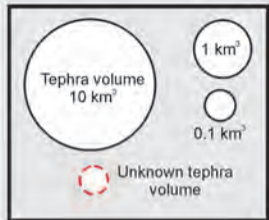


Mt. Burney



Reclus





18,000

14,000

10,000

6,000

2,000

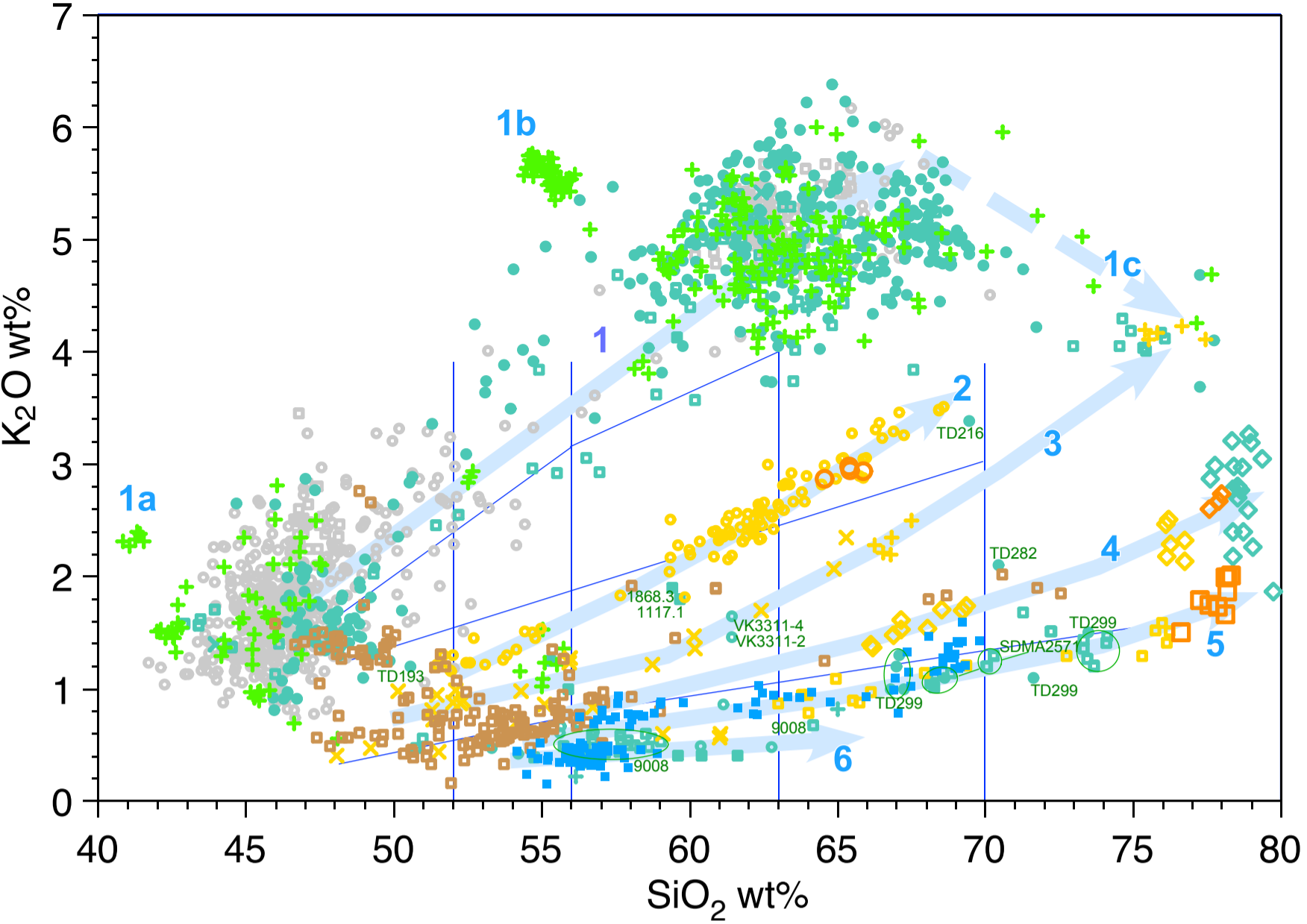
2018 A.D.

Eruption age (cal yrs BP)

Reclus

Mt Burney

Hudson



Antarctica	englacial	<ul style="list-style-type: none"> + MBL-NVL + Fuji Dome × Taylor Dome □ Siple Dome ◇ WDC06A ● Vostok ■ Dome C ● Talos Dome 	Peri-Antarctic	<ul style="list-style-type: none"> ■ South Shetland ■ South Sandwich
	ice cores	<ul style="list-style-type: none"> ● Hudson ◇ Reclus ■ Mt Burney + Aguilera × Fueguino-Macá-Cay 		South America
	off shore	<ul style="list-style-type: none"> ○ Andrill deep core □ gravity cores 		